Development of New Composite Materials for Secure Storage Units to Increase Burglary Resistance

by

Kai Roebbecke

A thesis submitted to the Graduate Faculty of
Auburn University
in partial fulfillment of the
requirements for the Degree of
Master of Science

Auburn, Alabama
May 5, 2018

Keywords: Burglary resistant safes, current state and advancements, ATM safes, Abrasive cutting, thermal cutting, impact resistance

Approved by

Bryan Chin, Chair, Daniel F. and Josephine Breeden Endowed Professor of Materials Engineering
Pengyu Chen, Assistant Professor of Materials Engineering
ZhongYang Cheng, Alumni Professor of Materials Engineering

Abstract

The aim of this research is it to find and develop new materials for secure storage systems with increased physical burglary resistance. The tests and evaluation of the materials takes place on the basis of the fulfilment of the common European and American standards, EN 1143-1 and UL 291. This would guarantee the certification of the developed materials. For the selection of potential safe materials, individual test procedures are devised to find the best materials in the most common burglary attack categories: Abrasive resistance, thermal resistance, and impact resistance. Comparable resistance values are determined for these materials and scientific relationships explained to consolidate the practical results. Composite solutions with the best performing materials of the tests are proposed to surpass the resistance values for commonly used safes. Additionally, improvement solutions for the developed concepts are given.

Acknowledgments

I would like to use this opportunity to express my gratitude to everyone who supported me during my research and preparation of my thesis.

First special thanks to my advisor, Dr. Bryan Chin, for his support and his expert knowledge sharing during my research. Thank you for letting me be part of this excellent research group and for giving me the opportunity to do my graduate thesis abroad. It was a pleasure to work with you and learn from this group. Hereby, I would like to express my gratitude to Songtao Du and Jun Chen.

Explicit thanks to the committee members, Pengyu Chen and ZhongYang Cheng, for their helpfulness. I also appreciate the help of Mr. Steven Moore and his trust for letting me use his workshop.

In addition, thanks to my sponsor for his financial support and especially for commissioning this research topic to Auburn University.

Furthermore, I would like to express my deepest appreciation to my family in Germany for support, in all respects, and for making this opportunity even possible. Last but not least, I would like to thank all of my friends for being a part of this amazing experience abroad, and for making it hard to leave. Special thanks to Madison Enebak for her huge support during my stay.

Table of Contents

List of Figures

1 Introduction

Secure storage units, or short safes, are commonly used for the secured storage of money, jewelry, or other valuable goods to prevent theft or damage. The scope of application is large and reaches from the private usage in small hotel safes to secure travel documents and money, to the large scale industrial usage of strong rooms in banks. All secure storage units, independent of their usage, have one feature in common, which is a strong body that cannot be improperly opened without the use of tools and an increased expenditure of time. One inconspicuous safe is included in every automated teller machine (ATM) to prevent the theft of money. Highly secured ATM safes are of a high interest to reduce the financial damage of ATM operators due to theft. In this research thesis, solutions to improve the ATM safety will be proposed, however improvements made for ATM safes can be transferred to the use in other secure storage units.

ATMs are sometimes afflicted by crimes of improper theft of money. Here, the crime can be of a fraudulent nature, or of a physical nature. Fraud attacks, also referred to as indirect attacks, are the unlawful gain of money without damage and physical harm of the ATM or to the involved people. Fraud attacks can involve, for example, card skimming, card trapping, or the manipulation of ATM software. Physical attacks, also referred as direct attacks, combine crimes where

brute force is used to open the safe, or to rob the refill personnel. To counteract physical and fraud attacks, several safety precautions are installed into an ATM. These precautions can be classified as active or passive precautions. Active precautions are electronic, mechanical, and measurement systems that intervene when a crime is detected. These can be sensors that detect attacks in progress and set off an alarm, explosive gas neutralization systems, or intelligent banknote neutralization systems that make the currency unusable etc. [8][9][10]. Passive precautions do not take action and are meant to withstand physical attacks for as long as possible. Reinforced metal safe bodies, explosion absorbing materials, and anti-ram raid bollards are examples for passive precautions [8]. Herein, the thesis is focused on the development of passive materials for the safe body to increase resistance in the event of physical attacks. Nowadays, traditional ATM safe bodies are made of steel and/or concrete [8]. Furthermore, the most common standards for physical certification and evaluation of ATM safes state that new ATM safes must meet an equal resistance of 25.4 mm thick steel [2]. These concepts allow improvements of ATM safes with higher burglary resistance. For the development of potential improvements, technologies and methods used for physical ATM crimes are understood. This knowledge allows the construction of test methods and devices to evaluate the new developed materials. A high thermal, abrasion, and impact resistance of the safe material is fundamental. The potential of stronger engineered safes, in terms of reducing the stolen money, is shown in the following.

2 ATM Crime Statistics

Nowadays, Automated Teller Machines are essential in regions where banks are not on site, or to enable financial transactions outside business hours. To enable customers' access to, for example, cash withdrawal, more ATMs are installed worldwide. Rapid growing numbers of ATMs can be recorded in Asia, the Middle East, and Africa, reaching a total number of over 4 million worldwide this year [5]. A negative side effect of this development is the unmanned operation of the ATMs which allows some people to feel favored to illegally enrich themselves by robbing the ATMs. Statistics also show that the willingness of an individual to rob an ATM has increased in the past years. Europe had a mildly increasing number of 400,000 to 420,000 (5 % increase) ATMs since 2010. However, the total number of ATM crime incidents increased by almost 65 percent (see Figure 1) [6][7]. In Figure 1, it shows that the fraud attacks strongly increased with the years, but for the physical attacks there is no trend noticeable over the last 12 years. However, the physical incidents increased by almost 50 percent when comparing 2014 (1980 incidents) with 2016 (2974 incidents). In 2015, there were 2,657 physical incidents.

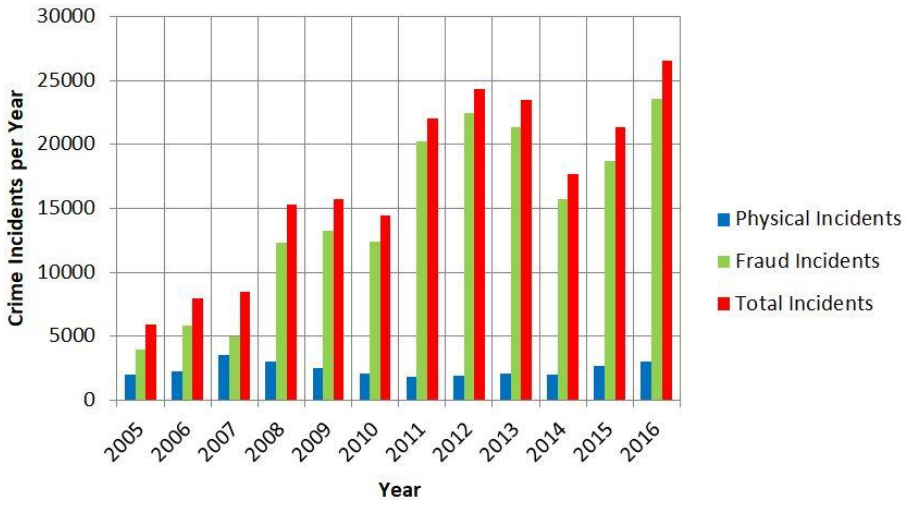

Figure 1: ATM crime incidents per year separated into physical incidents (blue) and fraud incidents (green). The red bars indicate the sum of physical and fraud incidents as the total crime number. The collected data are represented for the European Union. [6][7]

Also, the stolen money during physical incidents increased by almost 100 percent in 2015 and 2016 compared to 2012, 2013 and 2014, which is shown in Figure 2. Simply put, fraud attacks make up the main percentage of the total stolen money.

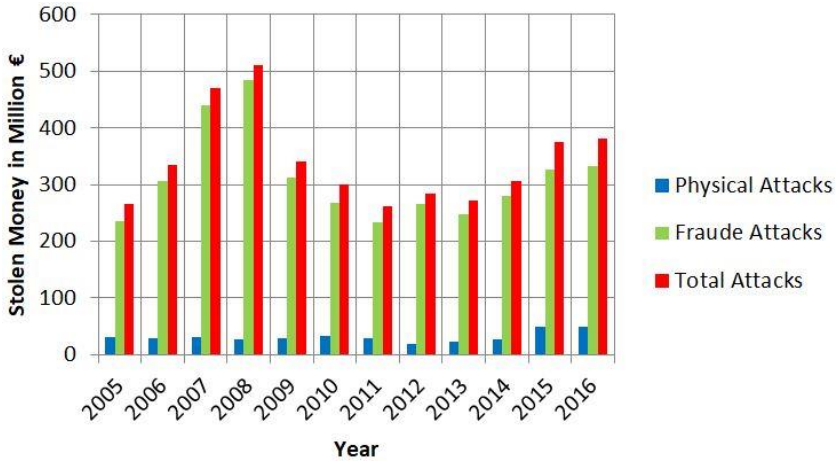

Figure 2: The stolen money per year separated into money stolen during physical attacks (blue), and money stolen during fraud attacks (green). The red bars indicate the sum of physical and fraud incidents as the total stolen money. The collected data are represented for the European Union. [6][7]

In 2014, there were 1,980 reported physical attacks in Europe. Figure 3 shows the classification into different types of attacks.

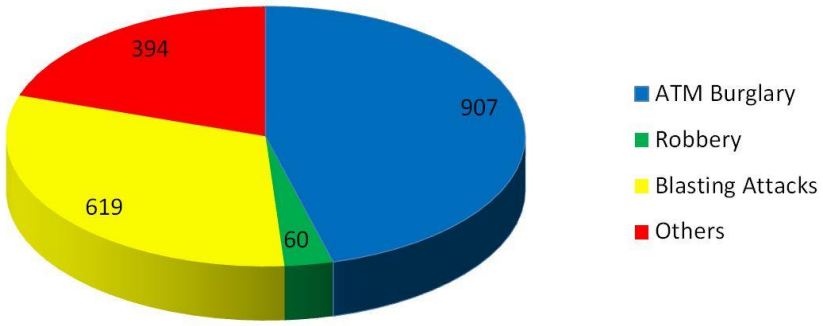

Figure 3: Types of physical attacks in Europe in 2014. ATM Burglary (blue) indicates attacks that use brute force to open the security container body, robbery (green) represents attacks where the refilling personal is robbed, blasting attacks (yellow) describe attacks with solid or gas explosives, and others (red) indicates attacks of cash trapping and vandalism. [6]

Sixty of the 1,980 attacks led back to robbery, where the personnel refilling the ATM is robbed. 394 other incidents were caused by robbery other than during cash refill, cash trapping, or by vandalism. 1,526 incidents can be directly traced back to the attack of the security container body of the ATM, whereas 619 attacks are implemented by solid explosives or explosive gas mixtures. The other 907 attacks directly on to the security container body of the ATM are caused by ripping it out, in-situ safe attacks and brute force, which can be referred to the term as burglary. A closer look at the money losses caused by these physical attacks in 2014, shows the importance of a strong protective engineered ATM safe. The losses were recorded to be about 27 million Euro. 1,317,499 € (5 %) induced by robbery of the refill personal and vandalism/cash trapping. The other 25,326,518 € (95 %) can be split into 2,071,596 € by explosive attacks, and 23,254,922 € by burglary. The losses are indicated in Figure 4.

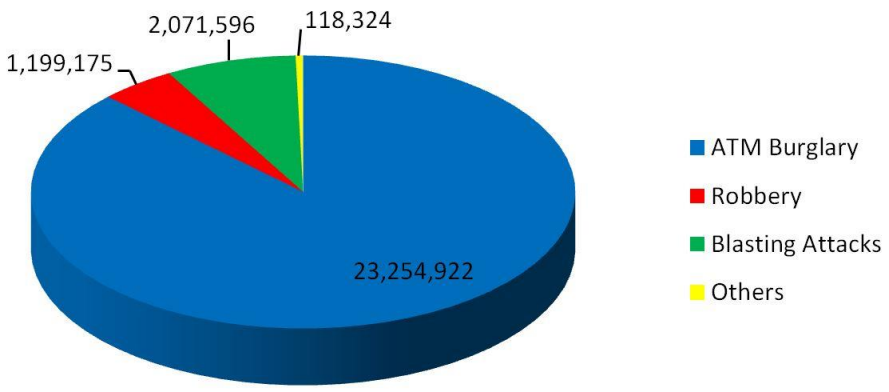

Figure 4: Amount of stolen money by each type of physical attack in the EU in 2014. [6]

Herein, newly develop materials with increased resistance to burglary for ATM safes can limit this loss of several millions in Europe and all over the world where 24/7 cash withdrawal is present.

3 Literature Review

As mentioned before, a high physical and passive resistance of an ATM safe is achieved with a strong safe body that withstands physical attacks of any kind for as long as possible. The literature is very modest on the specifications of strong safe bodies. Materials, compositions and structure of these safe bodies are rarely mentioned as well as research literature that focuses on the development of safes. Some information is gained from consultancy services like the ATM Industry Association (ATMIA), which publishes security guidelines for the ATM involved industry [8]. Metal especially steel and concrete are mentioned here [8]. Additionally, standards of ATM safes and non-ATM safes are helpful by giving steel of a certain thickness as minimum requirements of the safe body [1][2]. A closer view into the standards is given in the following chapter. However, a comprehensive insight into the accomplishments of safes is gained from patents that were published in the last 40 years. Here, patents are found that are focused on the functional parts of a safe such as the door anchoring, door hinges, locking mechanisms, and self-sealing jambs that prevent the penetration of hot gasses [11][13][14][15]. Patents also address the structural assembly of a safe, which can be, for example modular or a spaced-apart concentricity of an inner and outer wall which reduces the heat exchange. Nevertheless, the most publicized patents for safes and ATM safes describe the usage of concrete composite materials for the body structure. Cast-able concrete, often Portland cement, with

aggregates is cast into a sheet metal shell and cured afterwards [16][17][18][20]. Fibers of steel and polypropylene of the dimensions 10 mm – 80 mm and diameters of 0.3 mm – 1 mm are added to increase the compressive and tensile strength as well as rebar mats of bar diameters up to 16 mm [16-20]. Here, the compressive strength can reach 55 MPa to 75 MPa [17]. Another used additive is fused and sintered aluminum oxide of maximum sizes of 25 mm to 50 mm, with the purpose to resist abrasive cutting attacks [16][18][19]. Anchors attached to the steel sheets are interlocked into the concrete which prevents the separation of the two components [18]. A patent from 1983 added to this composite concrete/steel material a copper plate that should resist oxy-acetylene torch attacks [16]. Absence of concrete based safes, a dense carbide composite is published. Boron carbide and silicon carbide are infiltrated by molten silicon to form a dense structure to resist abrasive attacks [21]. A metal based patent from 2017 presents a modular safe with a double structure of carbon steel and high hardness armor steel [22]. The double structure is chosen to simplify the fabrication since the high hardness armor steel is difficult to shape [22]. However, the high hardness steel prevents penetrations of several tools [22]. Another, patent submitted by the Lockheed Martin company, is a safe with a layered structure of two hardened steels for inner and outer walls, an abrasive layer, thermally conductive layer and an insulating layer [23]. The abrasive layer is a composite layer with silicon carbide particles and resists cutting tool attacks. The insulating layer is of a porous ceramic filled with water. Low heat conductivity and the vaporization of water reduces the heat transfer from the outside to the inside.

Between the abrasive layer and the isolation layer is the thermal conductive layer out of copper that dissipates heat rapidly. The inner hardened steel layer is protected when heat is applied to the outer hardened layer with a cutting torch [23]. All developments and ideas can be used for ATM safe and are often indicated as such. However, the evaluation and the performance of these patents are missing. Merely two of the patents stated resistances of burglary in terms of times and rating tests from standards [19][20]. Herein, the development of testing and evaluation methods for new safe materials is mandatory. Standards for the evaluation of ATM safes are present and are used for this purpose.

4 Evaluation and Certification of Safes

To prevent the unauthorized removal of currency, valuables, and data burglary, resistant safes have to fulfill certain requirements which are specified in national and international standards. These standards imply the classification of safes with different grades of resistance, the resistance category of safes needed for the certain application, and the methods of test for resistance to burglary. Furthermore, the classification of the safes allows the comparison of safes of different manufactures. Certification processes are introduced to confirm the compliance of the burglary resistance of the safe. The established standards and certification bodies are mainly limited to those of the European Union and the United States, but these standards are often used in worldwide markets. Leading European associations are the ESSA (European Security Systems Association) with the European Certification Body (ECB), and the European Fire and Security Group (EFSG) with the certification bodies CNPP in France, VdS Schadensverhütung in Germany, and SBSC in Sweden [3][4]. The certification bodies in the European Union and the United States meet the ISO/IEC 17065:2012 (Conformity assessment – Requirements for bodies certifying products, processes and services). In the United States, certification is performed by the UL (predecessor: Underwriters Laboratories) with its own standards. The understanding of the United States and European standards is essential to develop new burglary resistant materials that are in compliant of certification.

Additionally, evaluation methods for newly developed materials can be found to prevent the testing of a whole safe. The standards and their evaluation methods, in terms of physical burglary resistance, are discussed in the following.

4.1 Standards of the European Union

The European certification process of burglary resistance takes place with the compliance of a few standards accepted by the European Committee for Standardization. The commonly used standards for the evaluation are:

- EN 1143-1 Secure storage units – Requirements, classification and methods of test for resistance to burglary – Part 1: Safes, ATM safes, strongroom doors and strongrooms
- EN 1143-2 Secure storage units – Requirements, classification and methods of tests for resistance to burglary – Part 2: Deposit systems
- EN 1300 Secure storage units – Classification for high security locks according to their resistance to unauthorized opening
- EN 14450 Secure storage units – Requirements, classification and methods of test for resistance to burglary – Secure safe cabinets

The standard EN 1143-1 regulates the classification and test methods of ATM safes and other safes for valuable goods. The standard clearly distinguishes between these two applications, since the ATM safe has to meet different requirements. For example, the ATM safe has to have openings for cables and to exchange money. A detailed study of the standard is suggested.

ATM safes are grouped into nine categories according to the grade of resistance to burglary. The resistance grades L and I (Roman one) are the categories with the lowest resistance, and grade VIII (Roman eight) is the category with the highest resistance. Every category is assigned with a resistance value (RU), a number that increases with increasing resistance from 30 RU for category L to 825 RU for category VIII. The test and evaluation of an ATM safe is performed by a team trying to open the test safe or test specimen. A test specimen must have similar fugues and joints like an ATM safe. During the test attacks the exploitation of the safe door, anchorages and openings is common. A safe is considered to be open when a small control gauge of a specific dimension can be passed through the opening (part breakthrough), or a bigger control gauge of a specific dimension can be passed through the opening (full breakthrough). Tools for the burglary test of an ATM safe are classified into four tool categories, A to D, whereas the damage causation in category D is the biggest due to the allowed weight of a hammer or allowed power consumption of a tool, for example. Furthermore, all allowed tools are noted with tool coefficients (*c* in RU per minute of usage) and basis values (*BV* in RU) which are used to calculate the total resistance value (V_R in RU) of an ATM safe. The total resistance value (V_R) is calculated as follows:

$$V_R = \left(\sum t \cdot c\right) + \sum BV$$

Whereas *c* is the tool coefficient (RU/minute) of a specific tool, *t* is the time (minutes) of usage of the specific tool, and *BV* is the basic value (RU) of the

specific tool. The sum of all tool usages, until a breakthrough took place, gives the total resistance value in RU. If this value is higher than the laid down resistance value of a safe category (for example I to VIII), the safe can be certified in this safe category. Additional labels of EX and GAS can be added by successfully passed blasting tests with explosives (EX) or gases (GAS).

The following knowledge is gained from the standard to promote the development of new resistant safe materials:

- The standard provides information about which tools can be used and the specifications of these tools (weight, energy consumption, etc.) for the burglary test.
- Furthermore, with the resistance values of each safe category, the total time of usage for a single tool, or various tools, can be calculated. With the calculated usage time of a tool, an opening of the size of the control gauge should not be produced in regards of passing the requirements of a specific safe category.
- The number of hits with two handheld hammering tools is limited to 250 hits per tool attack.
- The body of an ATM safe of the category L does not have to be tested if the wall thickness is bigger than 24 mm with a tensile strength of 345 MPa, or the wall thickness is bigger than 12 mm with a tensile strength of 690 MPa.

These stated points are used to develop testing methods/devices and to evaluate the resistance to burglary for the new developed safe materials. [1]

4.2 Standards of the United States

The American certification process of burglary resistant safes takes place with the compliance of a few standards developed by the organization UL and approved by the American National Standards Institute (ANSI). The common used standards for the evaluation are:

- UL 291 Standard for Automated Teller Systems
- UL 687 Standard for Burglary-Resistant Safes

Different from the European standard (EN 1143-1), the American standard has separate standards for ATM safes (UL 291) and other Safes for valuable goods (UL 687). Due to the distinction, the American standard for ATM safes is less prescriptive in some sections compared to the European standard. For example, the differentiation between part breakthrough and full breakthrough does not exist in the American standard, and also control gauges are not used. In the American standard, an ATM safe is defined as open when the currency can be removed. Also, a detailed study of the Standard for ATM safes is recommended.

The UL 291 standard distinguishes between three categories of ATM safes according to their resistance to burglary and service hours. Category one is the business hour ATM with the lowest resistance. The business hour ATM is available during the service hours of another business under surveillance of responsible personnel, for example ATMs in stores. Category two is a 24-hour

ATM level 1, and category 3 is a 24-hour ATM level 2 (ATMs that are available at any time). A business hour ATM has to withstand a 2 minute noisy/damaging attack and a 5 minute quiet attack without releasing the money to be certified. The used tools should not be powered or exceed a length of 0.6m and a head weight of 1.4 kg. A category two 24-hour ATM (level 1) has to resist an attack for 15 minutes with tools of level 1. Level 1 tools include mechanical and portable electric tools, as well as hand tools up to a mass of 3.6 Kg and a length of 1.5 m. A category three 24-hour ATM (level 2) has to resist the same 15 minutes, but in addition to level 1 tools, level 2 tools can also be used. Level 2 tools include gas cutting processes of any kind with a limited total gas consumption of 28.3 m^3 during the burglary test.

The following information is gained from the standard to support the research:

- The standard gives information about the tools that are used for the burglary test. However, this information is not as specific as in the European standard, only restrictions to weight and dimensions are mentioned.
- The required times an ATM safe has to resist to an attack can be used to evaluate a newly developed material. A developed material has to resist this time of attack with each tool, or combination of tools. Also, worth mentioning, is that the material of the security container body has to resist a 5 minute attack, whereas the whole ATM assembly (24-hour ATM level 1 and 2) has to resist a 15 minute attack.

- Furthermore, the standard gives requirements of the thickness and tensile strength of the safe made of metal. The metal should be thicker than 25.4 mm, and should have an ultimate tensile strength of at least 344.7 MPa. Materials other than metal should have an equal or higher burglary resistance than 25.4 mm thick steel with a tensile strength of 344.7 MPa.
- Business hour ATMs should have a wall thicknesses larger than 1.35 mm for Steel and 1.91 mm for brass or aluminum.

Also, these stated points are used for the comparison of safe materials and to develop testing methods/devices for new ATM materials. Due to the low safety and resistance requirements of the business hour ATM, research is conducted for the 24-hour ATMs. [2]

5 Test Methods for Safe Materials

For the development of new materials with a high resistance to burglary, materials that are commonly used and the new materials for safes have to be tested and evaluated under certain conditions that are similar to the most common burglary attacks. Here, the statistics and standard for ATM safes are helpful to find and categorize the common burglary attacks. The standards EN 1143-1 and UL291 give information about the tools that are commonly used for burglary, and the statistics in Chapter 2 give information about the frequency of the attacks. Other literature here is modest. By analyzing the type of tools and statistics, the main requirements of a safe can be categorized into three properties:

- Impact resistance; a high impact resistance is connected with the ability for elastic and plastic deformation to dissipate the energy of an impact without cracking and showing openings. High impact resistant materials complicate burglary attacks with striking tools, ram raids, gasses and explosives.
- Abrasive cutting resistance; a high abrasive resistance allows the materials to withstand penetration and erosion caused by hard and sharp tools. A high abrasive resistance counteracts attacks with grinding, sawing and drilling tools.

- Thermal cutting resistance; the thermal cutting resistance is important to reduce the melting and burning of the safe material. A high thermal cutting resistance impedes attacks with cutting torches, plasma cutting devices, and exothermic cutting lances.

Materials that combine all these three properties are developed in this thesis. Other burglary attacks under exploration of weak points of the safe construction like fugues, openings, anchoring, and the disassembling with tools are not considered in the development since the new materials are not tested in the whole of a safe. The tests of parts save material costs and time. To test the materials in all three properties, a tool is chosen for each. The tools are selected with the standard EN 1143-1, as it provides the most detailed tool requirements. For each property, the heaviest and most damaging tool is chosen from each category. Therefore, for the impact test a hammer with a maximum head weight of 3 kg, a maximum moment of 25 Nm, and a length of 1000 mm is selected [1]. Additionally, a 3.6 kg hammer with a length of 1500 mm is chosen to include the standard UL291. For the abrasive cutting test, an angle grinder with the maximum power output of 2300 W is chosen, and for the thermal cutting tests an exothermic cutting lance system is used due to the highest generation of heat among the thermal cutting instruments [1]. For the comparability for safe materials used in the past and new developed materials, the standard UL291 gives assistance. As mentioned before, the standard describes that every safe material should have an equal resistance to burglary as 25.4 mm thick steel with a tensile strength of 344.7 MPa [2]. Steel with these requirements are evaluated

in all three resistant properties and used as a reference, which is compared with all other tested materials. A material performing better than the steel reference in all three properties can be considered as an alternative safe material. The following chapters will focus on the improvement of each resistance property.

6 Improvement of Safe Materials against Abrasive Attacks

As mentioned in the previous chapter, a high abrasive wear/cutting resistance hinders the penetration of saws, grinding power tools, and drilling machines. The abrasive wear caused by these three groups of potential burglary tools can be explained as the following: Two contacting materials, such as the safe body material and the material of the attacking tool, are pressed onto each other. The material of the tool, which is propelled, is tangentially moved to the other material and due to the movement, a force is caused between the materials [24]. This force and the surface pressure cause the tool, which usually has a hard, rough, and with a sharp surface, to scratch grooves into the softer safe material [24]. The softer safe material is removed in the form of loose fragments [24]. However, not only fragments of the softer material will occur, but also from the harder tool material with a macroscopic higher mechanical strength, which is attributed to the result of adhesive wear. The tool material can exhibit microscopic regions with low strength due to defects. Appearing shear forces can break off these regions [24]. On the contrary, abrasive wear will not occur to the tool material as long as it is harder than the safe material [24]. In conclusion, safe material should exhibit properties that resist abrasive wear and causes abrasive wear to the tool making it unusable. An experimental setup and tests to find these materials are discussed in the following.

6.1 Abrasive Cutting Test Device

The selection of an abrasive tool for the test is described in chapter 5. An angle grinder, as the most destructive tool among the listed cutting tools in standard EN 1143-1, is chosen. Here, a “Bosch 1994-6 A High Performance Large Angle Grinder” is used with an idle RPM of 6500, required voltage of 120 V, the amperage is 15 A. The used cutting wheel is made of resinoid bonded abrasives with the dimensions of Ø 230 mm x 3.2 mm (Brand: Klingspor, “Kronenflex C24 Extra”). The tool requirements of the standard EN 1143-1 are fulfilled. To evaluate and compare abrasive cutting resistant materials, an abrasive cutting device is developed that is not influenced by human contributions, such as expert knowledge, force, and functioning of the testing person. It is also mentionable that these requirements are opposite from the standards EN 1143-1 and UL 291, where the expert knowledge and functioning of the testing persons is decisive. For the device, a construction with aluminum profiles and a linear guidance is assembled. To ensure the repeatability, the angle grinder is attached to a stiff arm and a constant force pulls the test sample on the machine table, through the rotating blade [see figure 5]. The assembly is chosen to ensure that the deep immersion of the cutting wheel into the test sample cannot be simulated, but that the cutting to enlarge a hole with an already deep immersed cutting wheel can. This means the cutting is simulated in a parallel direction to the safe wall. The latter is easier to control, since the cutting surface area stays the same. Therefore, a constant surface pressure during cutting of 0.85 N/mm², for all tested materials, is used. The surface pressure of 0.85 N/mm² allows the cutting

through 25.4 mm thick carbon steel without significant lose of rpm. The high surface pressure is chosen because the cutting velocity increases with increasing surface pressure. The surface pressure is realized by a weight which is adjusted to the cutting surface area. Furthermore, the turning direction of the angle grinder and the movement of the samples is in the up-cut direction to reduce vibrations and canting. A pneumatic cylinder is attached to the machine table to facilitate the start and stop of cutting.

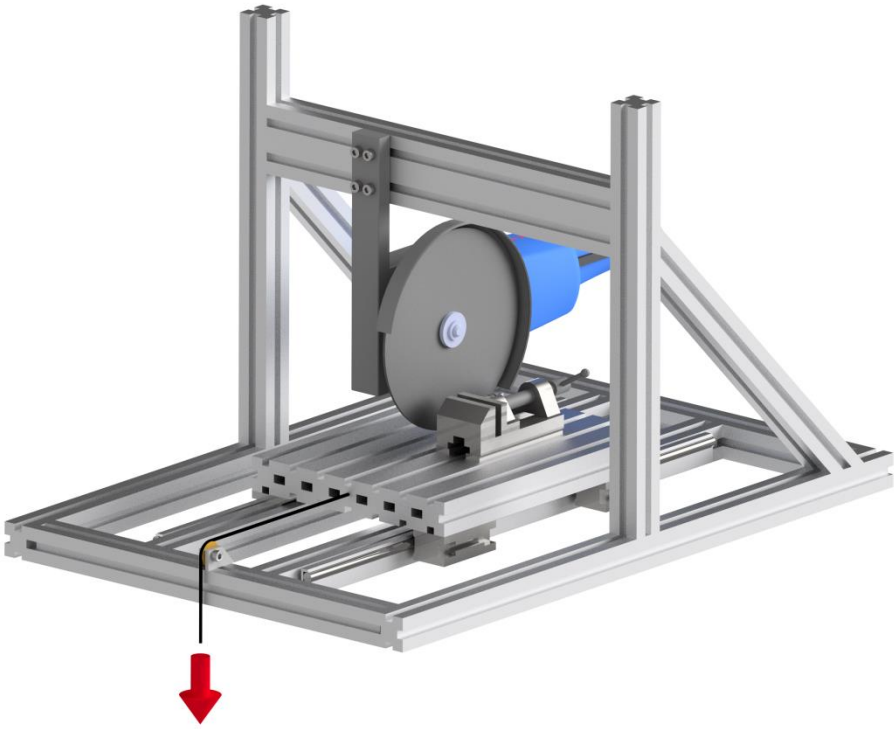

Figure 5: Abrasive cutting test device. For easy handling, the test samples can be fixed in a bench vice, which is attached to the machine table. The machine table is horizontally movable due to the linear guidance. A force indicated by the red arrow is realized by a constant weight. Test sample is clamped into the bench vice in the downright positon of the machine table. Then the attached weight force pulls the sample by the full length through the cutting blade.

Before a cutting test, the weight of the blade and the weight of the tested material are measured. For each test a new cutting blade is used to prevent uncertainties

of the measurements due to a damaged cutting blade from previous cutting tests. The measured parameters of the test are the weight loss of the cutting blade, the weight loss of the test material, and the total time of cutting. Furthermore, the densities of the cutting blade and the test material have to be known. With this data, wear volume ratio, removed volume from blade divided by volume loss of test material, is calculated. The removed volume per time is also calculated as the main indicator for the performance of the safe material. The volume is mainly used because the tested materials have strong varying densities, which would not allow the comparison of weights. For example, if 5 grams are removed from a polymer sample with the density of 2 Kg/dm^3, the cut would be four times longer compared to the removal of 5 grams from a steel sample with the density of 8 Kg/dm^3, concluding that the steel is four times better in resistance to cutting. First cutting trials showed that the geometry and thickness of the test sample has an influence on the cutting resistance. Thick and thin samples have a compulsorily different angle of cutting blade exit which influences the force distribution in the interface of rotation cutting blade and test material. Therefore, the samples should have approximately the same thickness for comparable results. It is defined that each sample should be 9.4 mm thick, but deviations of 20 % of the cutting blade exit angle are allowed. Material thicknesses of about 6.4 mm to 12.8 mm can be used. The tested materials are presented in the next section.

6.2 Materials for Abrasive Cutting Tests

Several materials are tested with the abrasive cutting device. Steels with different mechanical properties are tested to define the cutting resistance of a steel based ATM safe in accordance of the standards UL291 and EN-1143-1. Additionally, the potential to improve the resistance of commonly used steel safe can be determined. The tested steels are:

- 1045 carbon steel with a yield strength of 530 MPa and a hardness of Rockwell B90. The steel meets ASTM A108 and ASTM A29. Supplier: McMaster-Carr
- A514 alloy steel with a yield strength of 690 MPa and a hardness of Rockwell C30. The steel meets ASTM A514. Supplier: McMaster-Carr
- D2 tool steel with a yield strength of 345 MPa and a hardness of Rockwell B95. The steel meets ASTM A681. The steel is used untreated and hardened to Rockwell C65. Supplier: McMaster-Carr
- Low carbon steel with a yield strength of 370 MPa and a hardness of Rockwell B70. The steel meets ASTM A108. Supplier: McMaster-Carr

Other tested metals are:

- 309 stainless steel with a yield strength of 240 MPa and a hardness of Rockwell B95. The steel meets ASTM A240. Supplier: McMaster-Carr
- White cast iron with 12 % chromium and a hardness of Rockwell C55. The cast iron meets ASTM A532. Supplier: Clinch River Casting, Inc.

- Hardalloy 140 deposited on a 3 mm 1045 carbon steel. Hardalloy 140 are overlay electrodes that deposit a high chromium alloy steel with a hardness of Rockwell C55. Supplier: Hobart Brothers Company
- 110 copper with a hardness of Rockwell F65. The Copper meets ASTM B137. Supplier: McMaster-Carr

Promising candidates are ceramics which are used in the chipping production as high abrasion resistant materials. Furthermore, ceramics particles such as aluminum oxide, silicon carbide, and alumina zirconia are components of the used abrasive cutting wheels. Many tested ceramic materials are cutting tool inserts due to their availability and advancement. The following ceramics are tested:

- Aluminum oxide reinforced with silicon carbide whiskers (Grade: TC430) with a hardness of 2100 HV and a bending strength of 700 MPa. Supplier: Ingersoll Cutting Tool Company
- Aluminum oxide with titanium carbonitride (Grade: AB20) with a hardness of 2050 HV and a bending strength of 650 MPa. Supplier: Ingersoll Cutting Tool Company
- Aluminum oxide with titanium carbide (Grade: AB30) with a hardness of 2050 and a bending strength of 700 MPa. Supplier: Ingersoll Cutting Tool Company
- Aluminum oxide (Grade: AW120) Supplier: Ingersoll Cutting Tool Company

- SiAlON (Grade: AS500) which is an advanced silicon nitride ceramic with a hardness of 1800 HV and a bending strength of 850 MPa. Supplier: Ingersoll Cutting Tool Company
- Silicon nitride (Grade: AS10). Supplier: Ingersoll Cutting Tool Company
- Boron carbide. Supplier: Goodfellow

Composite materials can combine abrasion resistance with other mechanical properties that could not be achieved by a single material. The tested composites are:

- Cermet (Grade: PV3010), which is a combination of titanium carbonitride in a metal matrix out of cobalt. Supplier: Ingersoll Cutting Tool Company
- Cemented tungsten carbide (Grade: K10) Supplier: Ingersoll Cutting Tool Company
- Cemented tungsten carbide with 20 % cobalt. Supplier: Zhuzhou Tongda Carbide Co., LTD.
- Boron carbide particles embedded into a phenolic resin (Ground phenol-formaldehyde novolac containing hexamethylenetetramine) matrix. Supplier: Feldco International (boron carbide) and Plastics Engineering Company (phenolic resin)

6.3 Results of Abrasive Cutting Tests

The evaluation of abrasive cutting resistant materials for ATM safes takes place with the results of the wear volume ratio test and the cutting speed test. The wear volume ratio describes the ratio of the volume removed from the cutting blade to

the volume removed from the tested material. Materials that exhibit a high volume wear ratio cause a high material loss due to the cutting blade, whereas loss to the material itself is a comparably small amount of material. The loss of the cutting blades is greater than the loss of the material if the wear volume ratio is bigger than one. The wear volume ratio is an indicator of how likely the common burglary tools are damaged or worn out by the safe material. Materials with a high wear volume ratio can be considered as potential ATM safe materials. Figure 6 shows the results of the tested materials.

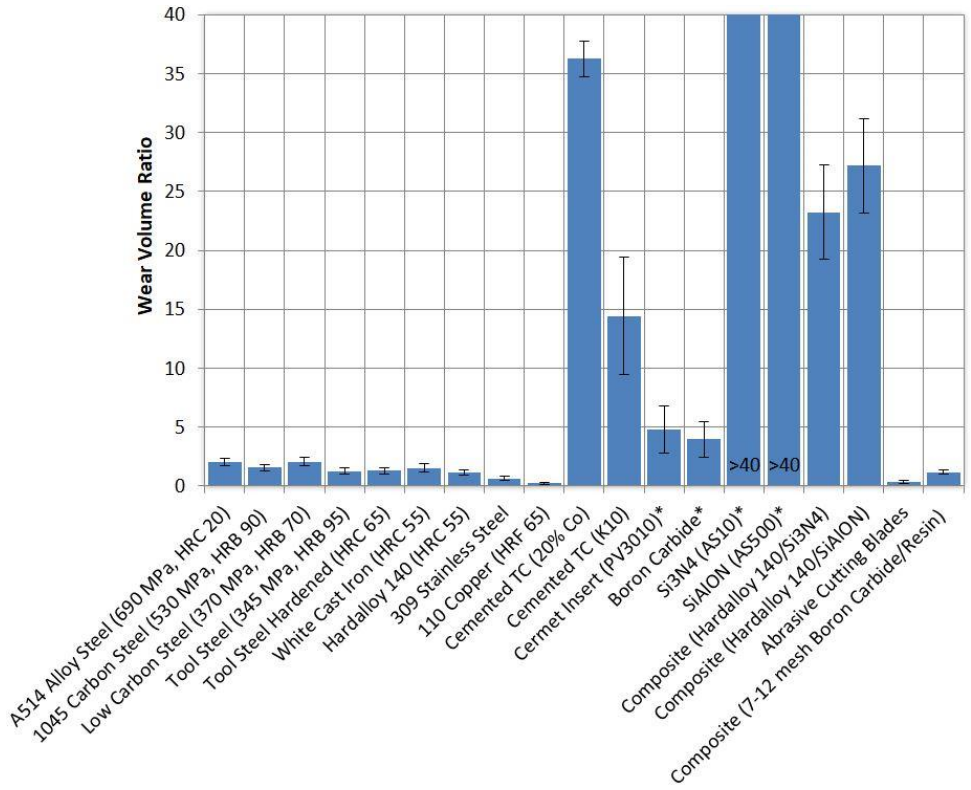

Figure 6: Wear volume of the cutting blade to the wear volume of tested material. Surface pressure of 0.85 N/mm² was not applied to materials indicated with "*".

It must be mentioned that all aluminum oxide compounds do not appear in the figure 6. These compounds all failed during the test. All aluminum oxide

compounds were too brittle to successfully pass the test. The thermal and mechanical load was too high, even for the aluminum oxide reinforced with silicon carbide whiskers (Grade: TC430) that exhibited advanced toughness properties. Cutting tests could not be continued with reduced surface pressure to minimize the thermal and mechanical loads. Additionally, materials indicated with a “*” were not tested with the full surface pressure of 0.85 N/mm². These materials also showed a tendency for brittle failure, but a reduced surface pressure allowed evaluation. Besides these changes to the process parameters, the data can be used to make a rough ranking of the abrasion resistance. Figure 6 shows that stainless steel, copper, and resting cutting blades have a wear volume ratio under one which makes them unsuitable for the use as ATM safe materials. The steels, as well as the chromium containing cast irons (Hardalloy 140, white cast iron), and the boron carbide composite showed similar performances with wear volume ratios between 1.2 and 2. However, the tested ceramics and the cemented tungsten carbides performed about 10 times better than the iron based metals. Since the surface pressure could not be realized for the silicon nitride based ceramics, they were embedded into the Hardalloy. The wear volume ratio stayed at a high level.

The wear volume ratio is not the decisive factor of a cutting resistant ATM safe. For example, burglars could replace worn out tools to counteract the increased wear caused by the safe material. Furthermore, the certification and evaluation into the resistance classes of the common standards takes place on the basis of the resistance time. Therefore, the removed volume of the tested material is

plotted over the time. Materials where the full surface pressure of 0.85 N/mm² could not be applied were not tested, as well as materials with a wear volume ratio smaller than one due to their low resistance. Materials with a low removed volume per time can be considered as potential materials for ATM safes. Figure 7 shows the results of the tests.

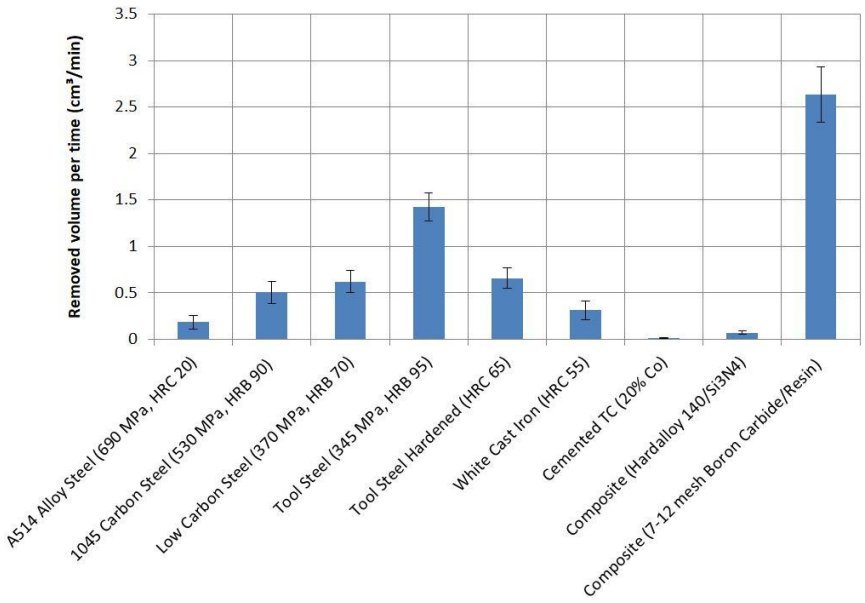

Figure 7: Removed volume per time of different materials as an indicator for the resistance time of an ATM safe.

Here, the changes between the different steels are more significant. Hard or hardened steels perform better than soft steels. It is worth mentioning that the cemented tungsten carbides and the silicon nitride composites show a similar high performance in the wear volume ratio tests. These materials perform several times better than the steel samples. The boron carbide/resin composite had an almost similar wear volume ratio compared to the other steel samples but had a significant higher removed volume per time. However, this composite is very light with a density of <2 g/cm³ and is therefore listed as a potential ATM material. The

theoretical aspects of the test results will be discussed in the following paragraphs.

6.4 Discussion and Theoretical Explanations of the Abrasive Cutting Test

From the results of the cutting tests, it was determined that there is a negative correlation between the wear volume ratio and the volume removed per time. Materials that cause a high wear to the cutting blade can just be cut with a high expenditure of time. A key factor here is the hardness of the materials. The tested materials that exhibited a high hardness or contained hard compounds had a high abrasion resistance. Researchers asserted that the abrasive wear is proportional to the hardness of materials, and also another study showed that the abrasive wear resistance of many pure materials is proportional to their hardness [24]. A high hardness counteracts the penetration of the abrasive grains in the cutting blade by reducing the wear. For example, the hard silicon nitrides in the Hardalloy composite, or the hard tungsten carbides in the cobalt matrix, are responsible for the good performance in both tests. The hardness and the participation of hard phases have also a positive influence on the iron based metals. Here, the removed volume per time was almost halved by hardening the 2D tool steel from HRB 95 to HRC65. The occurring hard martensitic phases led to the higher resistance [25]. The high strength steel A514 exhibited good performance due to quenching and tempering. The heat treatment combined with the small amounts of alloying elements led to a fine-grained microstructure with participations of hard bainite [26]. A hardness of Rockwell C30 could reduce the

abrasive wear. Furthermore, phases/participations of hard cementite (Iron carbide), and chromium carbide as they appear in the carbon containing steel, the Hardalloy, and the white cast iron increase the hardness, and therefore, reduce the abrasive wear. It was found that the microstructure of steels have an influence on the abrasive wear resistance and that the bulk high hardness of martensitic steel does not ensure a high abrasive wear resistance [27]. Here, multiple phase steels with hard and ductile phases can exhibit lower bulk hardness and a higher abrasive wear resistance. This could explain the poor performance of the unhardened and hardened tool steel in the tests [27]. However, iron based metals have been used in ATM safes for a long time. Patents reported about steel encasements and hardened steel armor plates. Due to the much better performance of the ceramics and ceramic containing composites, it will be focused on them.

The work of Archard exhibited that the materials with a very high hardness have the best abrasion resistances. However, some circumstances disprove this assumption for the abrasive cutting. First, researchers presented materials with a lower hardness and higher resistance than compared to materials with a higher hardness [28]. The behavior was found in, for example, the mentioned multiple phase steels and also ceramics. The elasticity expressed by the Young's Modulus of the materials was introduced to have an effect on the wear resistance. The hardness to Young's modulus ratio was established, which defines the strain to failure capability or limit of elastic behavior in the interface of contact and became an important factor describing the wear resistance and

durability of the materials [28][29]. Materials with a high H/E ratio deform more elastically instead of plastically [30]. Additionally, the H/E ratio also influences the friction between the tested material and abrasive grains of the cutting blade [25]. Here, the surface of the tested material can be deformed by piling-up or sinking-in around the abrasive grains. Materials that exhibit a high H/E ratio sinking-in is the preferred tendency of deformation [25]. Figure 8 shows an example of piling-up and sinking-in.

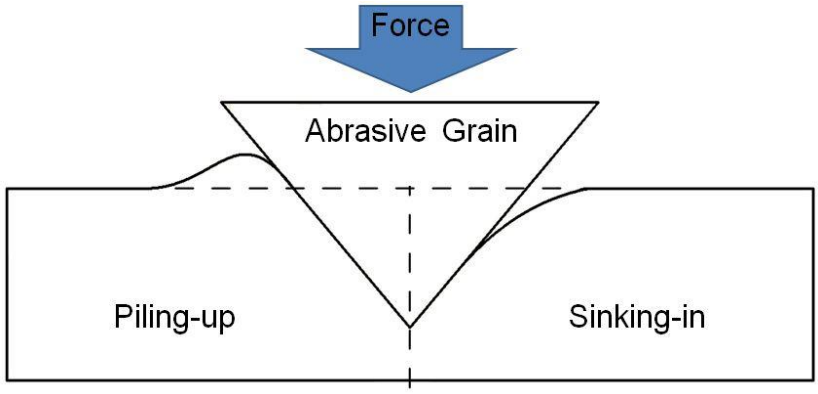

Figure 8: Schematic illustration of Piling-up and Sinking-in. The left side material indicates a material with a low H/E ratio, and the right side material indicates a material with a high H/E ratio.

Sinking-in is described to reduce the plowing force, which is the force that is needed to scratch or deform the material into the direction the abrasive grain is moved, resulting in a reduced friction between tested material and abrasive cutting blade [25]. Figure 9 shows the most common materials with hardness's over 700 HV plotted over the H/E ratio (Y-axis.). Materials with a high H/E ratio lay to the top, whereas materials with a low H/E ratio lay to the bottom. It can be seen that the silicon nitrides exhibit a high H/E ratio, which results in the good performance of the tests. The cemented tungsten carbides are ranged in the

lower area, which is due to the very high elastic modulus of about 510 GPa - 650 GPa (dependent on cobalt content), and a reduced hardness of 820 HV - 1500 HV due to the cobalt matrix [36]. Conversely, the high fraction of extreme hard embedded tungsten carbide with a hardness of 3400 HV are able to resist the abrasive cutting [36].

Other contributions that influence the wear of the tested materials are vibrations combined with high thermal stresses. Nearly all the mechanical energy of the cutting blade is converted into heat. Just a small fraction of the energy is converted into the surface generation and chip formation [31]. The generated heat is distributed into the cutting wheel, the atmosphere, the chips, and about 5% - 20% of the heat is transmitted into the material that is cut [32]-[34]. In the tested iron based metals, the cutting interface can reach temperatures of up to 800 °C, indicated by the occurring red heat. The high temperature reduces the hardness of the metals [34]. The yielding and plastic deformation of the metal in front of the abrasive grains to form chips is encouraged [31][34]. This hardness loss increases the wear. The heat build-up is mainly influenced by the thermal conductivity of the materials which causes problems of a different kind for ceramics [35]. Different from the metals, the hardness of the ceramics does not decrease significantly, but the low conductivities of the ceramics led to a heat build-up which caused high mechanical stresses in the ceramics [31][34]. Also, differently than metals, the ceramics are worn by mircocracking and fracture initiated by the occurring high stresses. This explains the poor performance of the Aluminum oxide samples and the bulk boron carbide, which could not withstand

this high thermal induced mechanical stress. To avoid these mechanical stresses, materials with a high thermal shock resistance are required. A high thermal shock resistance is achieved by materials with a high fracture strength, high fracture toughness, low elastic modulus, and low thermal expansion coefficient [37]. Thermal shock induced cracks can occur strength-controlled or toughness-controlled. The decisive effect whether the thermal shock results in a strength-controlled failure or toughness-controlled failure of the material is the thickness of the material [37]. Each material has a transition thickness where the temperature jump is equal for strength-controlled failure and toughness-controlled failure [37]. However, most of the transition thicknesses are at ranges lower than 2 mm, which leads to a toughness-controlled failure of ceramic materials with a thickness larger than 2 mm [37]. The maximum temperature jump of a toughness-controlled failure under extreme conditions is proportional to the fracture toughness K_{IC} divided by the elastic modulus E and thermal expansion α [37]:

$$\Delta T \propto \frac{K_{IC}}{E\alpha}$$

In figure 9 the thermal shock resistance is plotted over the X-axis. Materials with a high thermal shock resistance lay to the right in figure 9. Iron-based superalloys and some rare earth elements exhibit the highest thermal shock resistance, but do not have a high H/E ratio. Silica seems to have an overall good performance, but due to the low bulk hardness of 1000 HV it is also not suitable as a high cutting resistant material [36]. The appearance of Silica in the right to top corner

of the diagram indicates that there rightly should be a third axis of the bulk hardness to prevent misunderstandings.

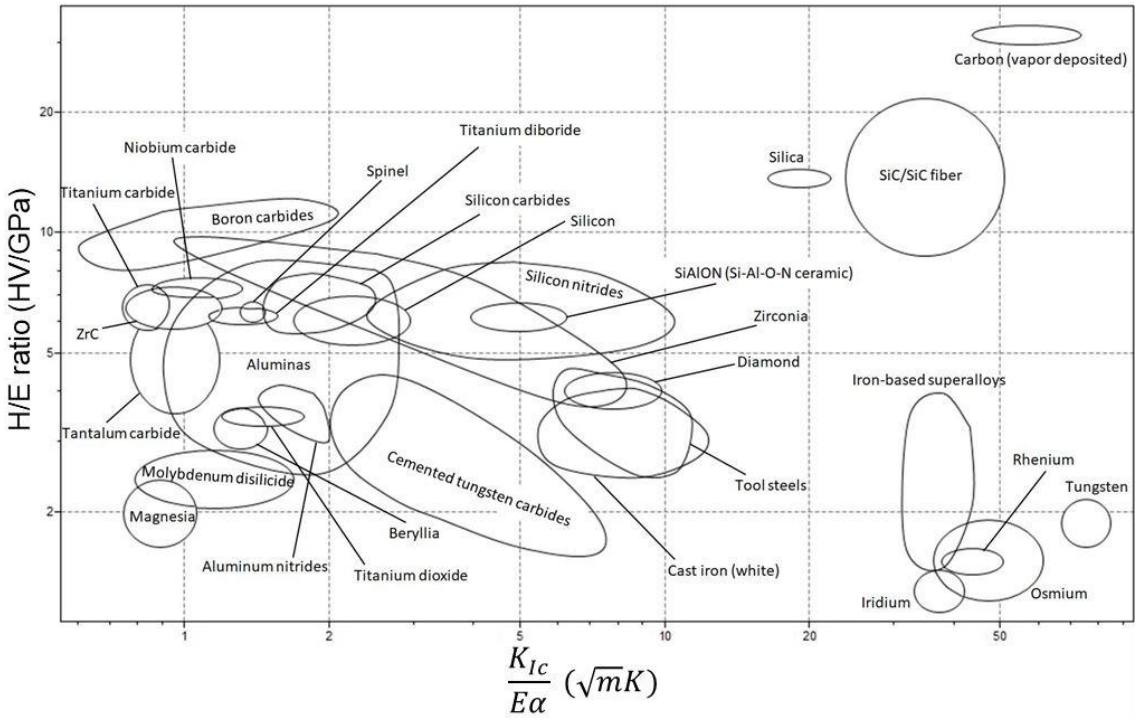

Figure 9: The H/E ratio representing the abrasive wear resistance over the thermal shock resistance for materials with a hardness over 700 HV [29][36][37].

Silicon carbide fiber reinforced silicon carbide also shows a good performance, but was not tested due to the exorbitant high price (up to 5500 $/kg) and poor availability making it unsuitable for the use in ATM safe materials [36]. The vapor deposited carbon is nanostructured single and multilayered material with almost no defects. The ideal structure and the small size explains the good performance. Researchers found that the size of the materials have an influence on the thermal shock resistance [38]. With decreasing size, the thermal shock resistance increases which could explain the better performance of the boron carbide particle composite compared to the bulk boron carbide [38]. Silicon

nitrides and the cemented tungsten carbides have the highest thermal shock resistances among the materials in figure 9 with a sufficient hardness.

6.5 Conclusion of the Abrasion Cutting Tests

A device to measure the abrasive cutting resistance of several materials was developed. The materials that exhibit a higher cutting resistance than common steel were found, which is required for an ATM safe material to be certified. Hard phases in steel were found to enhance the abrasive cutting resistance in steel. Especially multiphase steels (for example TRIP steel) with martensitic and bainitic phases can increase the abrasive cutting resistance by maintaining a sufficient elasticity. Furthermore, silicon nitride and cemented tungsten carbide were found to have an outstanding abrasive cutting resistance that cannot be achieved with steel. The high hardness, high H/E ratio and good thermal shock resistance of these materials underline the good cutting test results. Several bulk aluminum oxides and bulk boron carbide would not be eligible due to a low thermal shock resistance, but since the thermal shock resistance increases with a decreasing material size, boron carbide particles were found to resist the cutting. Boron carbide particles with a high hardness and a high H/E ratio embedded into a phenolic resin could reach the resistance of steels. The market development of silicon carbide fiber reinforced silicon carbide with a high theoretical resistance should be watched. A decreasing price could make it a potential ATM safe material. Solutions with silicon nitride, cemented tungsten carbide and boron carbide particles will be developed. Further disciplines that an ATM safe has to resist will be discussed in the following.

7 Improvements of Safe Materials against Thermal Attacks

A high thermal resistance of ATM safe materials is desired to resist fire, oxy-fuel torch cutting, and exothermic (oxygen) lance cutting. A high resistance to fire is required to protect the interior from a surrounding fire, which is not necessarily caused by burglars. Flame retardant materials and thermally insulating materials are used to protect the interior of the safe from heat. However, oxy-fuel torches and exothermic lances are often used tools for burglary. These tools develop high temperatures and are able to melt or burn holes into the safe body. Oxy-fuel torches are mostly fed by an acetylene oxygen mixture due to the highest flame temperature (3200 °C) and flame power among the combustible gases [39]. An exothermic lance uses a solid fuel, such as a steel rod, through which oxygen flows. The steel rod is heated up to its autoignition temperature by an electric spark which ignites the steel in the oxygen atmosphere. The steel transforms into more stable oxides under emission of heat (exothermic reaction) [40]. Flame temperatures of about 3000 °C can be reached [41]. The produced heat powers the further combustion of the steel rod and provides heat for the cutting of the ATM safe. Both oxy-fuel torches and exothermic lances use the same principle of cutting the safe body. The developed heat of combustion is used to heat the safe material up to its autoignition temperature. Additionally, oxygen which is not used for the combustion of the acetylene or steel rod ignites the safe material under further production of heat (exothermic reaction). The occurring oxides and slag is

blown out by the oxygen pressure. Solutions to counteract these efficient burglary tools will be presented in the following paragraphs.

7.1 Thermal Cutting Test Procedure

The selection of a thermal cutting tool is described in chapter 5. A SLICE exothermic cutting system from the company ESAB was chosen as a tool for the cutting tests. SLICE exothermic cutting rods from ESAB with a diameter of 6.35 mm and a length of 560 mm were used for the tests. The cutting system needs an 80 psi oxygen supply and oxygen consumption of 212 L/min. The tool requirements of the standard EN 1143-1 and UL 291 are fulfilled. Similar to the standards, the oxygen lance is controlled by hand which is a factor of inaccurateness, since the cutting is influenced by the functioning of the testing person. The development of a device that guides the cutting lance as fast as the cutting front and balances the distance between tested materials and lance with the burning speed of the cutting rod was not necessary as long as some directives are respected that decrease the influence of the testing person:

- The cutting lance should always be held perpendicular to the surface of the tested material.
- The distance between the burning cutting lance and the surface of the tested material should be kept at a distance of 5-10 mm
- The cutting lance should be moved as fast as the cutting front moves. A complete cut through the whole thickness should be ensured before the lance is moved further. If the lance is moved too fast, the flame will not penetrate through the whole thickness.

A straight cut from an outer edge of the tested material is performed. The cutting length is measured as well as the cutting time. The length divided by the time gives the cutting speed, which is an indicator of the cutting resistance. Figure 10 shows the setup of the exothermic cutting with the mentioned directives.

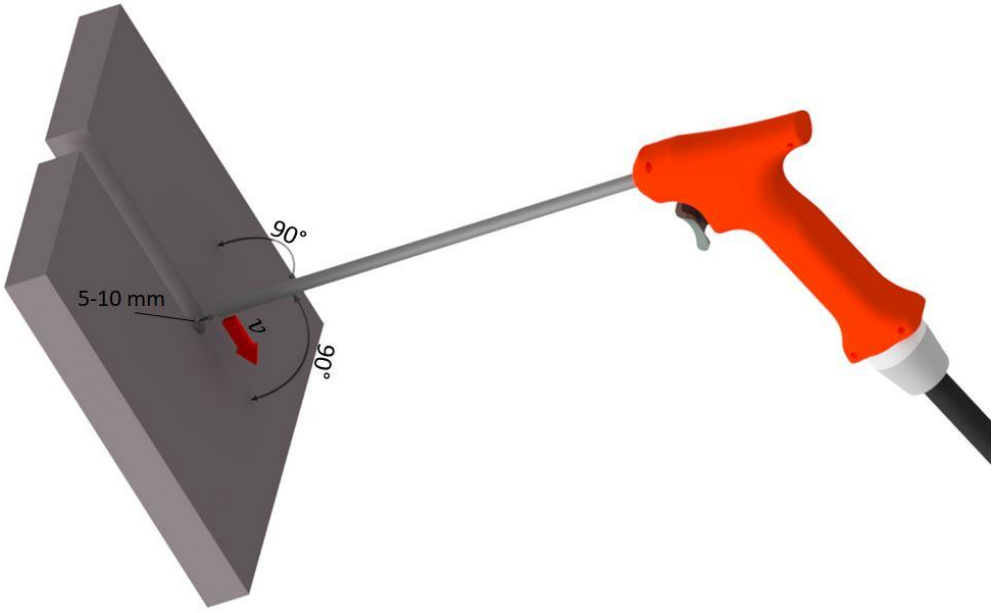

Figure 10: Schematic of the exothermic cutting with directives to ensure the repeatability. The red "gun" holds the burning steel rod and feeds the oxygen through the steel rod. "v" indicates the direction of the cutting speed. The rectangular steel sheet represents a test specimen with a cut.

A material that causes a low cutting speed has a high resistance to the exothermic cutting. The cutting speed is also dependent on the thickness of each tested material which, recommends that all materials should have the same thickness. Another option is that each particular material is tested with different thicknesses, which allows an interpolation of the cutting speeds over the thicknesses. The tested materials are listed in the following paragraphs.

7.2 Materials for Thermal Cutting Tests

Among the tested materials, steel and concrete is tested to set the reference cutting speed that must be achieved by the other potential ATM safe materials. Different metals are tested to evaluate the cutting speed:

- 309 stainless steel with a yield strength of 240 MPa and a hardness of Rockwell B95. The steel meets ASTM A240. Supplier: McMaster-Carr
- A514 alloy steel with a yield strength of 690 MPa and a hardness of Rockwell C30. The steel meets ASTM A514. Supplier: McMaster-Carr
- White cast iron with 12 % chromium and a hardness of Rockwell C55. The cast iron meets ASTM A532. Supplier: Clinch River Casting, Inc.
- 110 copper with a hardness of Rockwell F65. The Copper meets ASTM B137. Supplier: McMaster-Carr
- 6061 aluminum with a yield strength of 240 MPa and a hardness of Brinell 95. The aluminum meets ASTM B221. Supplier: McMaster-Carr

Ceramics are shown to have outstanding thermal properties in many high temperature applications. Therefore, ceramics are also tested:

- Low Thermal Expansion Alumina-Silicate Ceramic with a compressive strength of 170 MPa and thermal resistance up to 1100 °C. Supplier: McMaster-Carr
- Aluminum oxide ceramic with a compressive strength of 2060 MPa and a thermal resistance up to 1700 °C. Supplier: McMaster-Carr
- Boron carbide. Supplier: Goodfellow

Other tested materials and composites are:

- Graphite with a tensile strength of 40 MPa. Supplier: McMaster-Carr
- Cemented tungsten carbide with 20 % cobalt. Supplier: Zhuzhou Tongda Carbide Co., LTD.
- Boron carbide particles embedded into a phenolic resin (Ground phenol-formaldehyde novolac containing hexamethylenetetramine) matrix. Supplier: Feldco International (boron carbide) and Plastics Engineering Company (phenolic resin)
- Abrasive cutting wheel made of resinoid bonded abrasives. Brand: Klingspor, “Kronenflex C24 Extra”

7.3 Results of Thermal Cutting Tests

Among all the tested materials, the cutting speed dependence on the oxygen pressure is examined first. Exothermic cutting is performed with different oxygen pressures from 40 psi to 120 psi on a 25.4 mm thick A514 alloy steel. Figure 11 shows the cutting speed over the oxygen pressure. A stable burning steel rod could not be achieved with oxygen pressures under 50 psi. From this point, the cutting speed increases with the oxygen pressure by reaching its maximum at 120 psi.

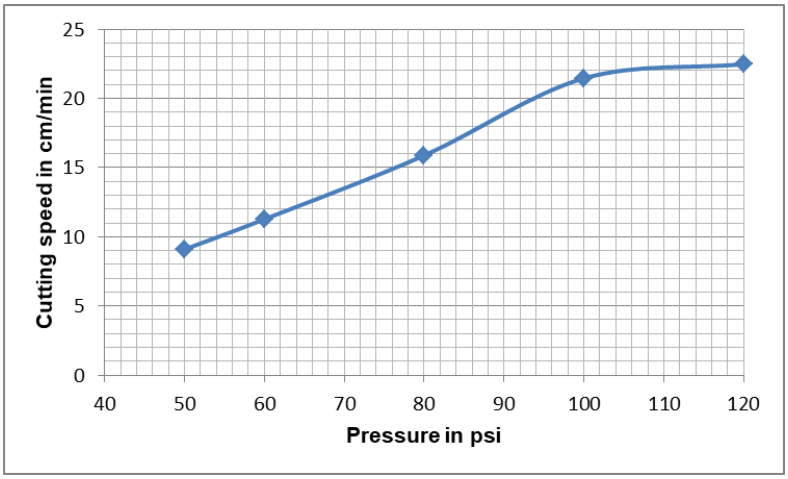

Figure 11: Exothermic cutting speed dependency on the fed oxygen pressure tested on a 25.4 mm thick A514 alloy steel.

Also, the total burning time of the steel rods increased with increasing oxygen pressure during this test. The burning time over the oxygen pressure is plotted in figure 12.

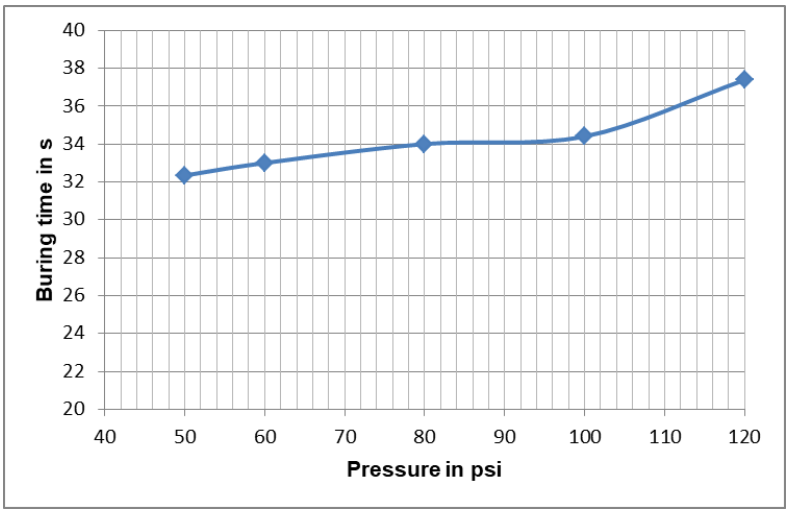

Figure 12: Total burning time of the steel rod dependency on the oxygen pressure timed during the cutting of 25.4 mm thick A514 alloy steel.

An increased burning time means that the total energy that is produced by the burning of the steel rod is spread over a longer time, which decreases the power

output of the thermal lance. Therefore, the power output increases with decreasing oxygen pressures.

Since the highest cutting speed was found for an oxygen pressure of 120 psi for the steel, it would suggest to test the other materials at a high oxygen pressure too. However, it was found that the cutting behavior of different materials varies from the cutting mechanism of steel. Therefore, the oxygen pressure was adjusted to the producer recommended oxygen pressure of 80 psi. The cutting speeds over the thickness for different materials are shown in figure 13.

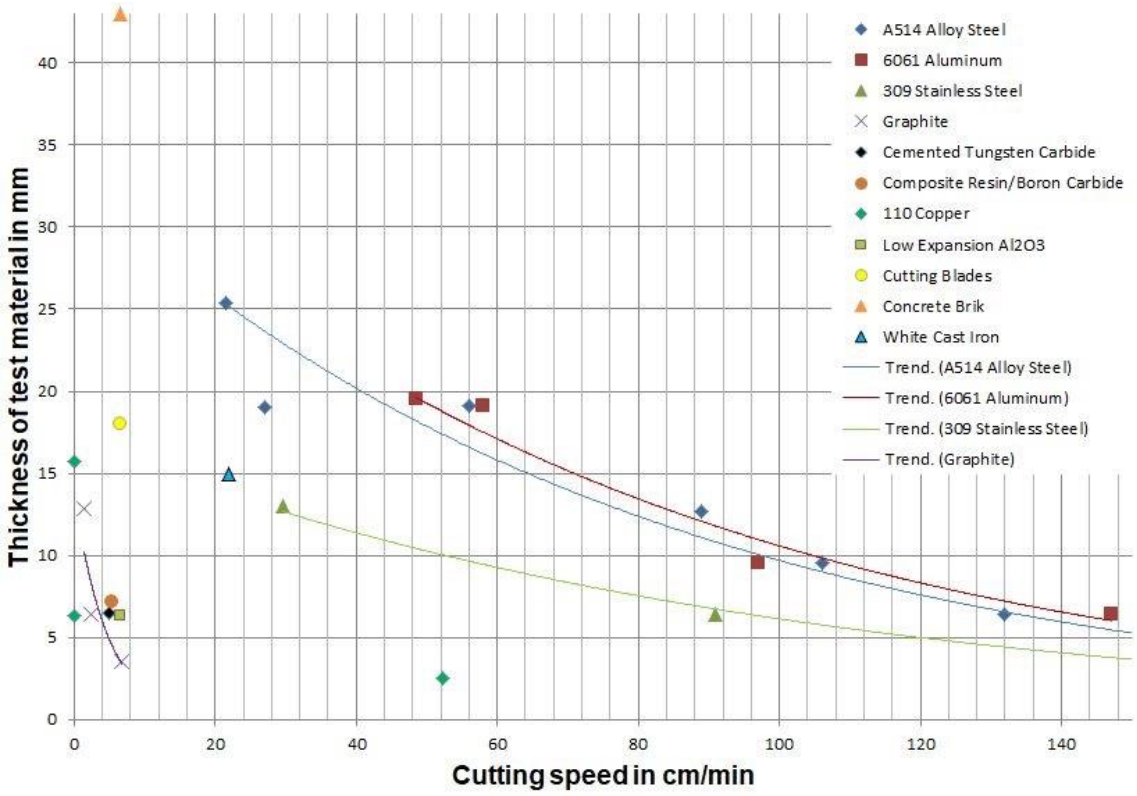

Figure 13: Cutting speed comparison for different materials dependent on the materials thickness.

Materials located in the left bottom corner of the diagram can be considered as potential ATM safe materials. These materials exhibit slow cutting speeds at low

material thicknesses. The resistance to thermal cutting is high at minimal material usage. In figure 13, it can be seen that the performance of metal based solutions, excluding copper, is modest. Aluminum and steel have the highest cutting speeds, whereas stainless steel and cast iron can be considered as more resistant to thermal cutting. Copper shows a much different behavior. At a thickness of 3 mm, copper has a much lower cutting speed than the other tested metals and at thicknesses over 6.3 mm the exothermic lance could not penetrate through the copper. Other than copper, the low expansion aluminum oxide, the cemented tungsten carbide, the phenolic resin composite, and graphite showed high resistances to exothermic cutting. The not plotted materials aluminum oxide and boron carbide could not be tested since they broke due to thermally induced mechanical stresses.

7.4 Discussion and Theoretical Explanations of the Thermal Cutting Tests

The exothermic cutting lance reaches temperatures that are able to melt or combust the ATM safe materials. Combustion of the safe material in the oxygen atmosphere contributes to a high cutting speed. Metals are special candidates that undergo such a combustion by producing solid condensed combustion products [40]. The rapid combustion appears at a specific temperature at which the heat release of the oxidation reaction exceeds the heat losses. This temperature is called the autoignition temperature. The autoignition temperature can be lower or higher than the melting point of a particular metal, which depends on a protective oxide layer. At temperatures lower than the autoiginition

temperature, an oxide layer is formed on the metal which reduces the speed of reaction since the oxygen transport through the oxide film is diffusion controlled. At a temperature where the oxide film loses its protection, the process changes from a diffusion controlled to a kinetic reaction rate controlled behavior [40]. Depending on the metal, this can happen before or after its melting temperature but usually appears in a temperature range close to the melting point. The ignition of copper occurs at about 1065 °C, which is lower than the melting temperature (1085 °C) [42]. Aluminum ignites at a temperature range between is melting temperature (660°C) and the melting temperature of the protective aluminum oxide layer [43]. Steel ignites at about 1350 °C, before the melting temperature [44]. Metals with a high autoignition temperature are favorable for the use in ATMs since higher temperatures over a longer time must be provided by the thermal cutting tools for the ignition. However, also after reaching the autoignition temperature and initiation of the combustion materials, properties can influence the cutting behavior. Metals that produce highly stable oxides during combustion exhibit high heats of formation and combustion [45]. The high heat of formation of those oxides further powers the combustion and causes a higher cutting speed. This explains the poor performance of aluminum in the cutting tests, which has a high heat of combustion (31.04 MJ/kg) compared to carbon steel (7.4 MJ/kg) and copper (2.45 MJ/kg) [46]. Furthermore, the reaction rate influences the cutting as well as the heat capacity of the reaction products and the thermal conductivity of the test material [45]. The heat capacity of the reaction products and the thermal conductivity of the test materials indicate how

much heat is dissipated from the main combustion zone. The reaction products make up a small percentage of this dissipated heat, whereas the heat dissipation of the bulk test materials can be so high that the autoignition temperature and melting temperature cannot be reached. The 6.3 mm thick copper showed such behavior. Copper has a high thermal effusivity which allows the copper to dissipate heat very fast. A high thermal effusivity e is given by a material with a high thermal conductivity k, a high density ρ, and a high specific heat capacity c_p [47]. The thermal effusivity e is calculated as follows:

$$e = \sqrt{k\rho c_p}$$

In figure 14, the thermal effusivity is plotted over the melting temperature of several elements. The thermal effusivity is the highest for pure elements and with increasing degrees of alloying, the thermal effusivity decreases. Besides copper, silver also has a thermal effusivity that could resist the exothermic cutting, but due to its high price it is not considered as a potential ATM safe material. The thickness and size of copper sheets installed into an ATM safe can be constructed so that they resist a specific time of a thermal cutting attack. This attempt will be used in the following chapter to design an ATM safe.

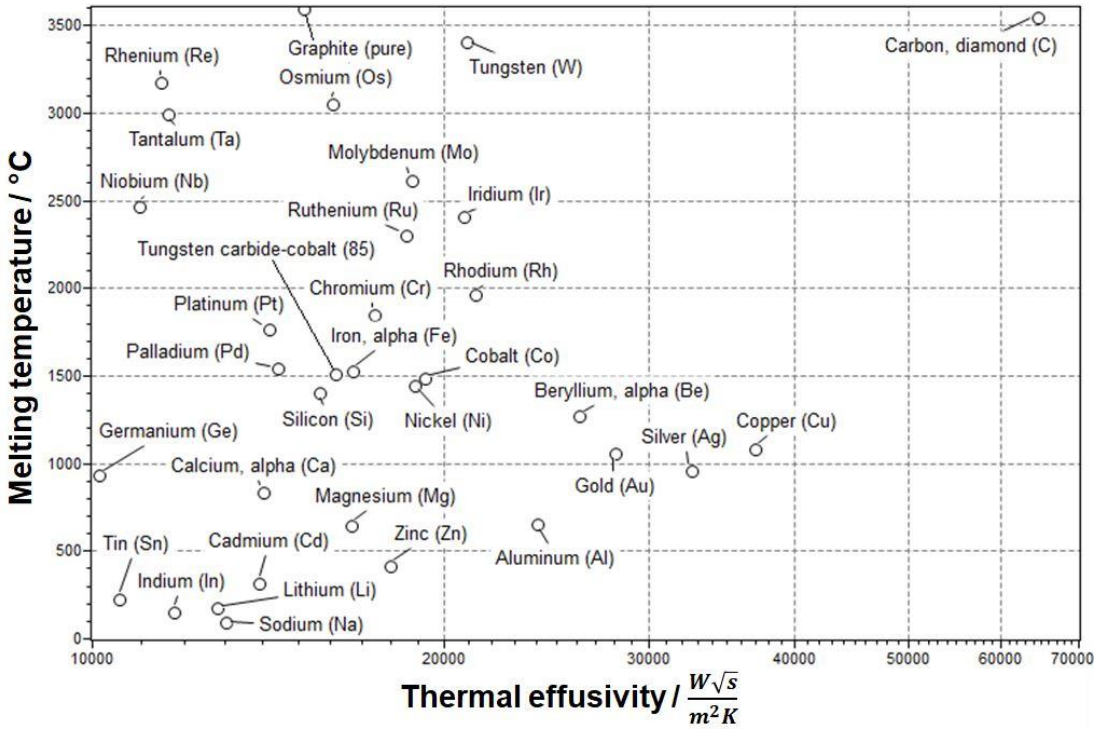

Figure 14: Thermal effusivity for several elements plotted over the melting temperature. The diagram allows an estimation of which elements and their alloys exhibit a high heat dissipation, and additionally are compatible with increased temperatures. Graphite and cemented tungsten carbide (85% tungsten carbide) are added additionally. [36]

The cutting speed through steel was found to be dependent on the oxygen pressure fed to the thermal lance. The higher supply of oxygen does not influence the autoignition temperature since the autoignition temperature is not dependent on the oxygen pressure [44]. Nevertheless, the higher oxygen pressure provides more oxygen to the combustion, which could favor the cutting speed. The main effect of the increasing cutting speed can be explained that the occurring reaction products are ejected faster from the combustion zone by the jet. On the contrary, the power output of the thermal lance reduces with increasing oxygen pressure indicated by the increased burning time of the steel rod. The energy provided by the burning steel rod is spread over a larger period

of time. This behavior can be explained by the fact that the increased oxygen flow rate through the steel rod has a cooling effect. Simulations showed that the oxygen temperature at the burning tip of the steel rod has a temperature of about 35 °C, whereas the burning steel rod tip reaches temperatures of about 1800 °C at proper oxygen flow rates [41]. An increased oxygen flow rate with an oversupply of oxygen that is not needed for the combustion of the steel rod would cause a higher heat dissipation from the steel rod tip which reduces the temperature. The reduced temperature leads to a decreased reaction rate of the steel rod. On the other hand, exothermic cutting with low oxygen pressures that just fed enough oxygen for the combustion of the steel rod produces the highest power output. This could favor the cutting of copper where high heats must be provided to counteract the heat dissipation in the copper.

Besides copper, graphite shows low cutting speeds at small thicknesses. The high thermal conductivity of graphite is one reason of the excellent cutting resistance. Another reason is the inert and corrosion resistant nature of graphite [48]. The carbon atoms are bonded with strong covalent bonds, which require high activation energies to break off [49]. Furthermore, the graphite consists of graphite crystallites in which graphene basal planes are stacked together. The crystallites only allow the oxidation decomposition on the outer edges, which strongly reduces the reactive surface area and inhibit the diffusion processes of oxygen into the crystallites [50]. Additionally, it was found that at temperatures below 800 °C, a protective oxide layer further reduces the decomposition [51]. Graphite is also not susceptible to thermal shocks due to the weak Van der

Waals forces between the graphene layers which balance tensions. However, these bindings are responsible for a weak tensile strength of graphene and a poor macroscopic hardness which complicate the use as an abrasion resistant material.

A good exothermic cutting resistance is also achieved by the phenol formaldehyde resin/boron carbide composite. A major portion of the good resistance can be assigned to the flame retardant phenolic resin. Phenolic resins have no melting point but do decompose at temperatures greater than 340 °C. From 340 °C to 600 °C some decomposition products are phenol, aldehyde, water, carbon monoxide, and carbon dioxide [52]. At temperatures greater than 600 °C, as the dehydration further proceeds, a carbon-like structure (char) is formed. The char is formed with a by-product of carbon monoxide. The char is declared as amorphous carbon and/or as a glasslike carbon [52-54]. With the formation of this carbon-like layer, the decomposition rate strongly reduces since the layer hinders the outgassing of flammable gases from the resin and hinders the entering of oxygen into the resin [52]. The boron carbide particles were found to support the thermal cutting resistance as well.

Low cutting speed at small thicknesses were also achieved by the cemented tungsten carbide with 20 wt.% cobalt. Cemented tungsten carbides have been used in the chipping industry as cutting tools where temperatures in an oxidizing atmosphere can reach up to 1000 °C [55]. Good oxidation stabilities and mechanical properties at elevated temperatures have been reported. However, temperatures in the exothermic cutting test surpass the temperatures where the

adequate mechanical properties are achieved. Nevertheless, the good exothermic cutting resistance can be associated with a high thermal effusively that dissipates the heat fast, and therefore a reduced peak temperature is achieved. Furthermore, cobalt and tungsten carbide have high melting points of about 1500 °C for cobalt and about 2800 °C for tungsten carbide. The autoignition temperature of cobalt is assumed to be slightly below the melting point, but self-heating of bulk cemented tungsten carbide has not been reported in the literature which further supports the high resistance to thermal cutting [56]. Oxide films were also found to protect the cemented tungsten carbide from further oxidation [55]. At temperatures up to 800 °C, a protective and dense $CoWO_4$ film is formed on the surface which appeared in a green/blue color around the cutting area [57][58]. At temperatures above 1000 °C, a more intensive oxidation of the tungsten carbide into the porous WO_3 was found, as well as the volatilization of WO_3 [55][59]. The final failure is predicted to be due to the liquefaction of the cobalt and the volatilization of WO_3, which formed a porous slag.

Bulk aluminum oxide and bulk boron carbide failed the thermal cutting tests due to poor thermal shock resistances. This behavior is in agreement with the abrasive cutting where the thermal shock resistances were also exceeded. The thermal shock failure cause by the exothermic cutting was of a much more severe extent than during the abrasive cutting. However, low thermal expansion aluminum oxide with a more porous structure could withstand the thermal shocks

but due to a poor tensile strength and hardness, this material is not suitable for the use of ATM safe materials.

7.5 Conclusion of the Thermal Cutting Test

A procedure was developed to evaluate several materials according to their exothermic cutting resistance. The tests showed that steel as a common used ATM safe material and a reference material for the certification of ATM safes does not exhibit a high thermal cutting resistance. Reasons for this behavior are the fast heat up to the autoignition temperature and the heat release due to self-combustion. Several materials were found to perform better than steel. In general, materials with higher oxidation stability than steel showed lower exothermic cutting speeds. Copper which has a thickness over 6.3 mm, were found to be the only metal (with an adequate price) that can completely resist the exothermic cutting, which is due to the high heat dissipation that does not allow temperatures to reach its melting or autoignition temperature. Also, the boron carbide/resin composite and the cemented tungsten carbide shows superior cutting resistance which makes them potential ATM safe materials as well. Good exothermic cutting resistances are achieved due to the formations of protective layers and the absence of self-heating in the oxygen atmosphere. Copper, the boron carbide/resin composite, the cemented tungsten carbides are selected as potential ATM safe materials with high thermal cutting resistances and undergo further investigation. Another reason for the selection, is that these materials also have adequate mechanical properties which were not the case for low expansion aluminum oxide and graphite that had high thermal cutting resistances. Solutions

for the combination of high thermal cutting resistance with a high abrasion resistance and a sufficient impact resistance will be presented in the following paragraphs for these materials.

8 Improvements of Safe Materials against Impact Attacks

An adequate resistance to impact attacks is a requirement of safe materials to prevent fragmentation and cracking of the safe body. During an impact, the high kinetic energy of a body colliding into the ATM safe is transformed into elastic and plastic deformation of the ATM safe in fractions of a second. Safe materials that are able to absorb the kinetic energies of several impacts are desired. The energy of weak impacts can be transformed into elastic deformation of the safe materials, which means that the atomic bonds are stretched and the atoms are able to return into their origin position. A high fraction of energy is emitted back to the impacting body and the other fraction of energy is dissipated into damped vibration of the ATM safe. The safe behaves similar to a spring and maintains this behavior as long as the stresses do not exceed the yield point. If the impact energy surpasses the elastic limit of the safe material, the occurring stresses will cause yielding of the material. The energy is absorbed by the plastic deformation of the safe material. The atoms and dislocations move in their preferred slip directions under production of heat, which is not reversible. The safe material remains deformed. In the plastic region, metals dissipate the highest amount of energy. When the plastic deformation of the safe material is exhausted, the energy will be dissipated into the formation of cracks. At this point, the currency in the ATM will be accessible. If the safe materials are of a brittle nature, then the energy dissipation due to plastic deformation will not occur. After reaching the

limit of the elastic deformation, these materials dissipate the energy into the propagation of cracks. The safe would then fracture into many pieces. It is mentionable that the energy dissipation of either the plastic deformation or crack propagation occurs simultaneously with the elastic deformation. This means that after the plastic deformation, for example, a fraction of energy is stored in elastic energy which is transferred back to the impacting body. As mentioned, the highest amount of energy is dissipated during the plastic deformation for metals. However, the ability of plastic deformation depends on the temperature and the strain rate during the impact. With a decreasing temperature the atoms and dislocations lose their mobility and the material becomes brittle. Also, with an increasing strain rate which indicates the deformation per time, the atoms and dislocations are not given enough time to move and the materials changes to a brittle behavior. In this chapter, ATM safe materials with adequate impact absorption will be investigated based on theoretical analyses, computer simulations and practical impact tests. [60]

8.1 Test Approaches for Impact Resistant Materials

The two standards, UL291 and EN 1143-1, are chosen to define the boundary conditions for the used tools in the impact tests. The standard EN 1143-1 allows the usage for automatic impact tools with a power of 1350 W and a limited single impact energy of 20 J. Furthermore, a hammer with a maximum head weight of 3 Kg and a maximum moment of 25 Nm can be used as an impact tool. The amount of impacts is limited to 250 hits with a two handheld impact device (large hammer). However, the standard UL291 allows the usage of a hammer with a

weight of 3.6 kg and length of 1500 mm. The number of hits is not limited. As a compromise between the two standards, the potential safe materials are tested with a 3.6 kg hammer falling from a height of 1500 mm which equals an energy of about 53 J (Nm). With a simulation software (Ansys Workbench 2018) the impact behavior of a full ATM body with the mentioned tools can be analyzed. Furthermore, the transition wall thickness where the safe changes from an elastic deformation to a plastic deformation can be defined as well as the maximum stress, deformation and strain rate. In addition to the simulation software, a material selection software (CES EduPack 2017) is used to choose materials with their properties that have a high energy absorption during an impact. To confirm or disprove the theoretical results, a drop tower equipped with an acceleration sensor (Company: PCB, sensitivity: 0.5 mV/g, range: 10000 g) and an oscilloscope device (Tektronix TDS 3014B) is used for practical tests. Due to a limited height of the drop tower device, a falling hammer with a height of 1500 mm cannot be processed. Instead, a hammer weight of 5.4 kg falling from a height of 1000 mm is chosen to keep the impact energy equal to 53 J. The impactor (tup) is a steel bar with a diameter of 32 mm, which has a semi-sphere at the impacting surface. The test sample is supported by a support ring of 76 mm in diameter. The configuration allows test samples with a rectangular shape and edge lengths of 100 mm, whereas the sheet thickness of the test samples can be variable. Figure 15 shows the drop tower.

Figure 15: The drop tower test is used to confirm computer simulations and theoretical approaches. Plastic deformations of the test samples can be compared with the computer simulations.

8.2 Results and Discussion of Material Selection

To define the impact requirements of an ATM safe, a finite element method is used to analyze the behavior of a whole safe body under an impact. The finite element simulation is chosen because of the fast adaptability which allows the tests with different wall thicknesses and different constructions of the ATM safes without physical construction and tests. For the simulation, a common low strength constructional steel (non-linear) with a yield strength of 250 MPa is used

for the body of the ATM safe. Additional chosen parameters for the simulation are provided by the engineering data source of Ansys:

- Density: 7850 Kg/m³
- Young's modulus: 210000 MPa
- Poisson's ratio: 0.3
- Bulk modulus: 167000 MPa
- Shear modulus: 76923 MPa
- Tangent Modulus: 1450 MPa
- Specific heat: 434 J/(Kg*K)

Steel is the choice of comparison according to the standards. The safe body is designed as a hollow cube with a side length of 450 mm and a variable wall thickness. However, the exact size of the safe is not known, as well as constructional weaknesses. For example, doors and openings are not taken into account. The bottom side of the safe body is fixed in all directions to simulate a firm anchoring to the ground. A cylinder with a weight of 3.6 kg simulates the hammer impacting with a velocity of 5.43 m/s which equals an energy of 53 J and is in agreement with the standards. The hammer hits centered into a lateral safe body wall. The figure 16 shows the simulation view. The simulation view (figure 16) shows a safe body with the wall thickness of 10 mm. A wall thickness of 10 mm turned out to be the transition thickness where the steel changes from an elastic/plastic deformation to solely elastic deformation. The maximum equivalent plastic strain reached a value of 0.00195 mm/mm in this simulation.

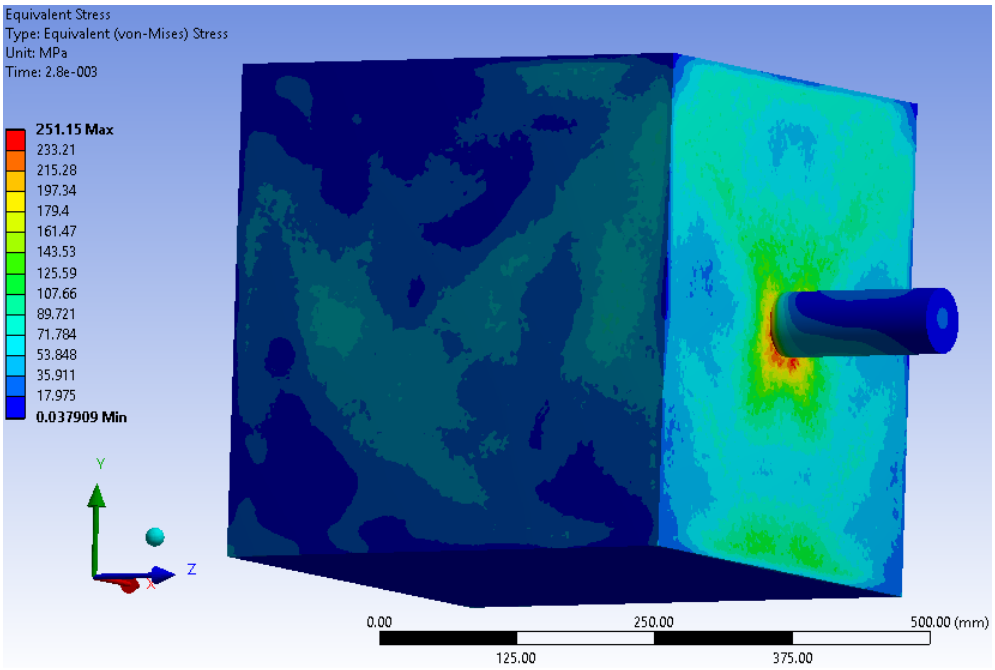

Figure 16: Simulation view of equivalent stress at maximum deformation. The stress maximum lies on the inside of the safe wall, where the surface is stretched the most. Stresses pervade the whole safe body resulting in vibration and further energy dissipation. The bottom face's movement is suppressed in all directions.

From this point, decreasing wall thicknesses caused an increase in the plastic strain. Nevertheless, the thickness of 10 mm might sound very low since wall thicknesses up to 25.4 mm are proposed in the standards. This can be explained by the fact that the impact in the simulation occurs centered onto a side wall which allows the wall to transfer a lot of the impact energy into elastic deformation. If the impact takes place on specific constructional parts for example the door or openings, an increased wall thickness might be required. Further, the impacts can be aimed onto the edges of the safe to exploit the notch effect of the underlying right angle. These weaknesses are of a constructional nature and will be neglected in this research.

To decrease the calculation effort of the simulation, a comparison model with a reduced number of mesh points is developed. For this, the safe wall that is mainly involved in the impact is separated from the rest of the safe body and is individually supported as similarly as possible to the original setup. It was found that when the movement of the edges of the separated wall, essentially a sheet with the dimensions of 450 mm x 450 mm x 10 mm, is prevented into the z direction, the results will be in agreement with the original safe design. The movement of the edges in x and y direction are free. The reduced model showed similar stress levels and a slightly increased plastic strain of 0.0026 mm/mm, which is due to the stiffer support. Figure 17 shows the simulation setup with decreased number of mesh points. With the simpler model, the mesh can be refined to increase the accuracy. The plastic deformation as well as the strain rate is simulated for different wall thicknesses. The strain rate, plastic strain divided by time, is an important factor during impacts since a strain rate that is too high can cause the brittle failure of the material, which would result in reduced impact energy absorption [60]. As a simulation results, the equivalent (von Mises) plastic strain is plotted over the time. The maximum strain rates for wall thicknesses below 10 mm rose from 20 s^{-1} for a 9 mm thick wall to 63 s^{-1} for a 3 mm thick wall. The total plastic strain reached a maximum of 0.012 mm/mm for the 3 mm thick wall for a single impact.

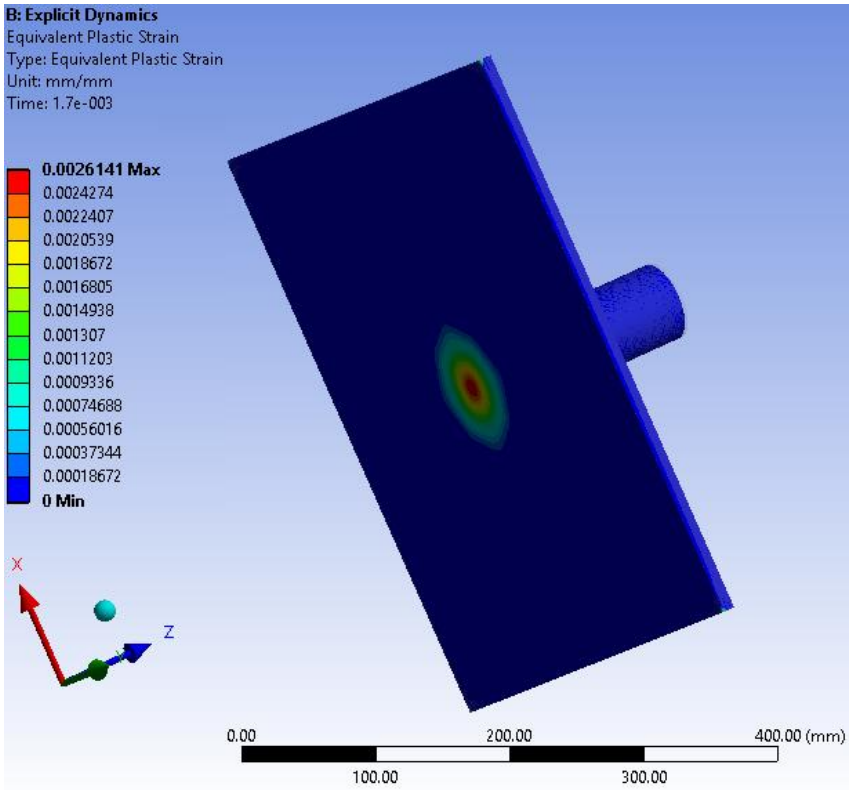

Figure 17: Simplified model with decreased number of mesh points, but with refined mesh. The simulation view shows the inside wall of the safe where the stresses reach its maximum simultaneously. The highest plastic deformation is reached here. The movement of the edges of the plate are limited into the z direction, but movable into x and y direction to reproduce the original support.

These impact simulations have analogies to the practical and standardized charpy impact test, where the energy absorption of a probe is measured under high strain. Differences of the charpy impact test are that a notch changes the stress state into a triaxial stress, which further suppresses the plastic flow and favors brittle failure [61]. The safe wall does not contain notches and a biaxial stress state will occur, but high strain rates can still cause a brittle failure [61]. The maximum strain rates in the simulations reached about 63 s^{-1}, which is considered to be in the intermediate strain rate range [62]. Previous studies on various steels showed that at these strain rates the plastic deformation is not or

not significantly reduced [63-65]. A study on various auto-body steel sheets investigated that the strain rates up to 200 s^{-1} do not reduce the plastic deformation. Steels with tensile strengths of 280, 350, 400, 640 MPa were tested [64]. Another study on advanced high-strength steel sheets reported a 14% decreased plastic deformation at a strain rate of 567 s^{-1} compared to a quasi-static strain rate [65]. However, in the intermediate strain rate range an increase on the tensile strength was determined [63-65]. Especially low strength steels showed a higher strain rate sensitivity since the tensile strength increase was bigger than for high strength steels [64]. The results of the studies are based on tensile stress-strain curves produced at different strain rates. The stress-stain curves also provide information on the energy dissipation, which is of high interest in this research. The area under a stress-strain curve indicates the energy dissipation into elastic and plastic deformation. In Figure 18 the area is marked. The energy dissipation can be estimated by trivial materials properties: the maximum strain until failure, the yield strength and the (ultimate) tensile strength.

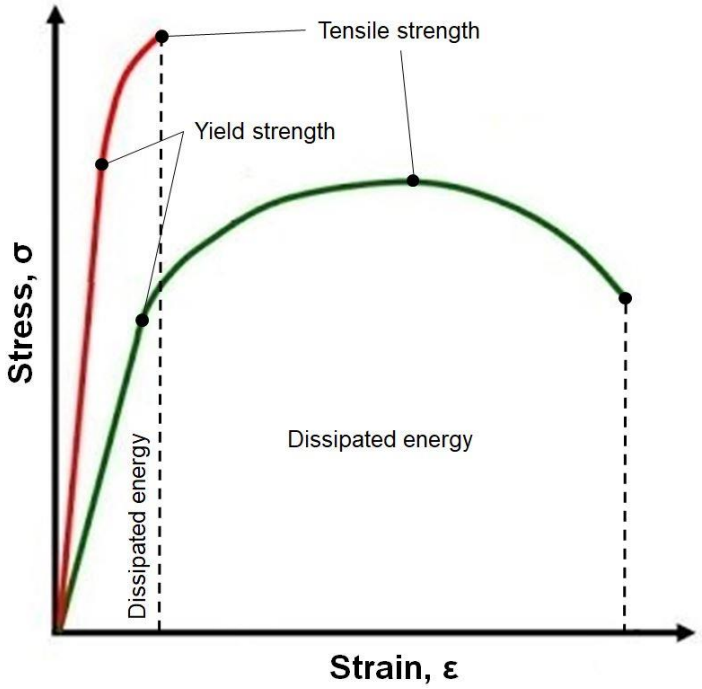

Figure 18: Stress-strain (tensile test) curve of a brittle probe and a ductile probe. The curve can also be interpreted as a force times distance curve, and therefore indicates the dissipated energy during the tensile test. The area under the respective curves, limited by the dotted line, shows the dissipated energy.

Since the simulation results and the previous studies are in agreement that these properties are not significantly influenced by the strain rate, a material selection software can be used to define materials with these favored properties. Materials with a high tensile strength and/or yield strength, as well as a high strain enclose a large area under the stress-strain curve defining a high energy dissipation during an impact. Figure 19 shows the yield strength vs. the strain for material groups. Material groups that lie to the right top of the figure 19 are favorable for the use as ATM safe materials since the energy absorption during an impact is the highest without fracturing and releasing the money.

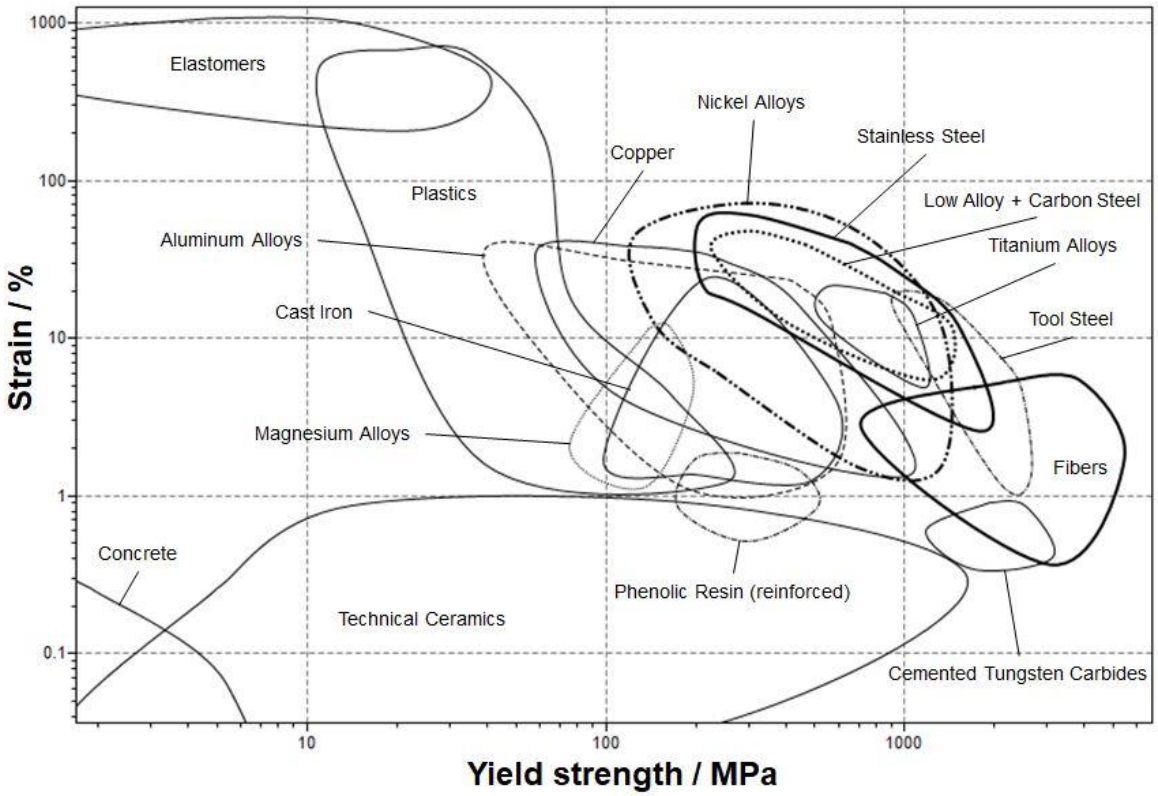

Figure 19: Strain vs. yield strength for different material groups. Yield strength times the strain gives a rough estimation of the energy dissipation during an impact at low strain rates. [36]

It is conspicuous that metals fill the right top of the diagram which is due to the nature of the metallic atomic bonds. Valence shell electrons are shared between the metal atoms, forming the so called “electron gas”. The electron gas produces a non-directed negative space charge which pulls the ions together. If the atoms are moved during plastic deformation, the electron gas ensures that the repulsive forces between the ions are smaller than the attraction forces [66]. Many material properties of metals can be transferred to the electron gas, for example, the high thermal conductivity of copper [66]. On the other hand, ceramic materials have covalent atomic bonds where the direction and distance between the atoms is fixed. If a ceramic material is plastically deformed, the order of the atoms will be

destroyed which leads to strong repulsive forces between the atoms and the material fails brittley [66]. This explains the poor strains of the technical ceramics in figure 19. Good impact performances can be expected from nickel alloys, stainless steel, low alloy steels and carbon steels. For example, TWIP (transformation induced plasticity) steels, as well as TWIP (twinning-induced plasticity) steels, are used in the automotive industry as high strength and high strain steels to improve the crash performance of cars [64][67]. Additionally, fibers show very high yield stresses at adequate strains. Due to the high yield stresses, fibers are able to dissipate high amounts of energy in the elastic region. One main reason for the high stress levels of the fibers is the size. Due to the thin structure of the fibers they have a statistical low probability of containing defects and stresses nearer to the theoretical cohesive strength can be reached [60]. New developed fibers have a tensile strength up to 5800 MPa and strains of 3.5 % (PBO Zylon fibers, Toyobo Co., LTD.). The good impact resistance of fibers has been proven in bullet resistant vests. However, the disadvantage of fibers is that they are flexible and need to be embedded into a matrix to form a stiff construction.

As mentioned before, the charpy impact test is a method to measure the energy dissipation. However, plastic deformation is limited and an amount of energy is dissipated into fracturing of the sample during the charpy impact test. For the fracturing, the atomic bonds have to be severed which needs energy. If the elastic limit (brittle materials) or the plastic limit is exhausted, a safe material will fail due to crack propagation. A high resistance to fracture expressed by the

fracture toughness is desired to further increase the energy dissipation. Here, previous studies found a correlation between the fracture toughness and the charpy impact energy [68][69]. This means that a material with high fracture toughness exhibits increased energy dissipation during an impact and fracture. Also, a materials selection software is used to choose potential ATM safe materials with appropriate fracture toughness's (see figure 20).

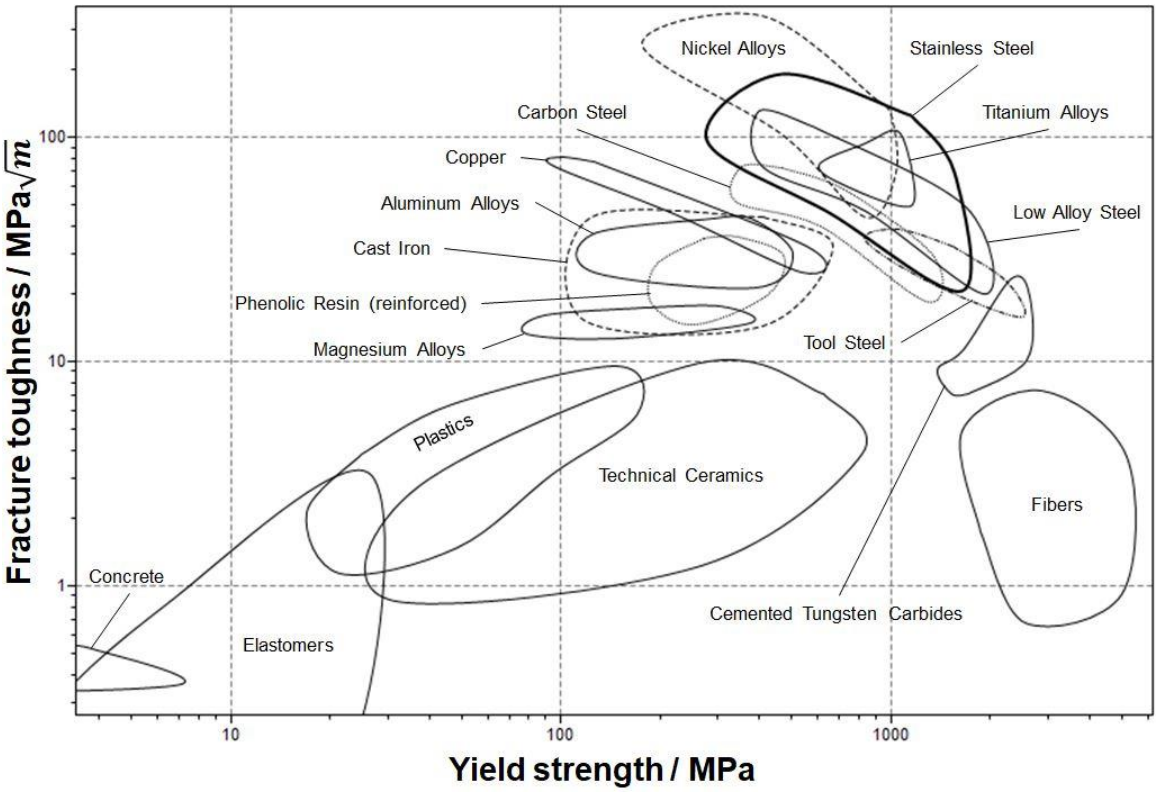

Figure 20: Fracture toughness vs. the yield strength for several material groups. A high fracture toughness is associated with an increased energy dissipation during fracturing. [36]

Material groups that lie to the top of the figure 20 show excellent fracture toughness. Not surprisingly the material groups that showed good performances in the evaluation of figure 19 also exhibit superior fracture toughness. In general, high toughness can be reached with the optimal combination of ductility and

strength, which was evaluated in figure 19. This explains the good overall performance of the metal groups. Furthermore, materials with adequate ductility can counteract the crack propagation by plastic deformation at the crack tip, which is restricted for materials with poor ductility. [60]. Moreover, the critical flaw sizes for metals are much larger compared to engineering ceramics and concrete [70]. The highest fracture toughness have nickel alloys followed by stainless steels, low alloy steels, titanium alloys and carbon steels.

Last, but not least, the simulation model and theoretical approaches are reviewed with practical impact tests. As the previous simulations demonstrated, an ATM safe with a steel thickness of 6 mm is able to resist the impacts with small plastic deformations. To confirm the theoretical results the drop tower test is used. In accordance to the figures 19 and 20, a high strength low alloy steel 5160 with a yield strength of 670 MPa and a thickness of 6.3 mm (Supplier: McMaster-Carr, Steel meets ASTM A689) is tested. Since the drop tower test setup differs from the initial simulation models, a new simulation model is developed for the comparison. The practical drop tower tests confirmed that the steel with its thickness is sufficient to withstand 250 impacts (limited impact number by standard EN 1143-1) without failure. The permanent deflection in the middle of the steel plate was 2.5 mm. The simulation result showed a stronger deformation due to a stiffer model, which means that the impact energy cannot be transferred to other components. In the praxis, impacts and vibrations are transmitted to other components due to a more complex setup. Furthermore, damping is

neglected in the simulation model. Figure 21 presents the simulation result after one impact.

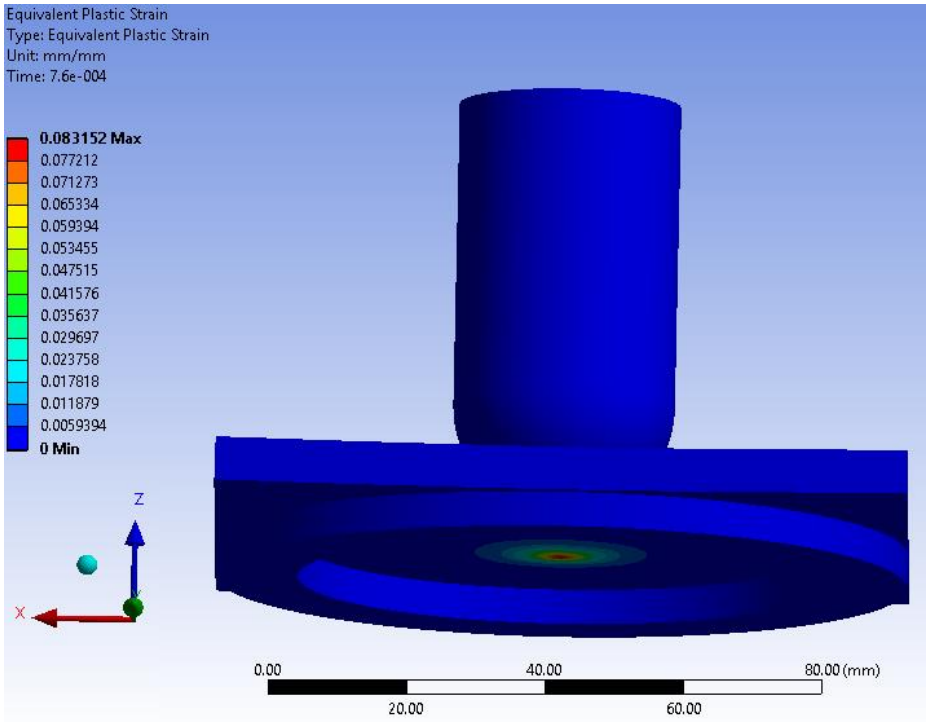

Figure 21: Simulation results of the drop tower test. Plastic strain and remaining deflection are more pronounced in the simulation due to a stiffer setup. The remaining deflection in the middle of the plate is about 0.6 mm after one hit. Less energy is dissipated by elastic deformation, which results in higher plastic deformation, and therefore in a high strain rate of about 285 s^{-1}.

8.3 Conclusion of the Impact Approaches

Theoretical and simulation methods were used to define ATM safe wall thicknesses that can resist the impact tools specified in the American and European standards. A safe wall out of a constructional steel (yield strength: 250 MPa) with a thickness of 6 mm showed an adequate impact resistance without plastic deformations surpassing the strain limit. To further improve, the impact resistance materials with an increased impact energy absorption are

needed. Those tough materials are characterized with a high yield and tensile stresses, as well as high ductility and high fracture toughness. Thousands of materials were evaluated according these properties with a material selection software. The results indicated that metals, especially iron based metals, have superior energy absorption properties during impacts. These have already been used in the automotive industry to improve crash performances. The simulation results and the material selection have been confirmed in practical drop tower tests where a high strength steel with a thickness of 6.3 mm could withstand the 53 J impact over 250 times. The common ATM standards require a resistance comparable to 25 mm thick steel. However, this comparison does not seem to address the impact resistance since smaller wall thicknesses offer a sufficient protection against the specified tools in the standards. However, the standard EN 1143-1 proposes a wall thickness of 12 mm if the steel exhibits a tensile strength of greater than 690 MPa.

9 Development of Composite Materials with a Good Overall Performance

In the three previous chapters, potential ATM safe materials were evaluated according to the three most common tool categories used in burglaries and specified in the standards. In summary, a burglary resistant ATM safe has to withstand abrasive attacks, thermal attacks, and impact attacks. The evaluation results stated the best performing materials for each category. An ATM safe should be made of the material performing the best in each category. However, there was no material showing an average high resistance in all three tests, which is due to the controversy of the requirements. For example, a hard ceramic material can exhibit excellent abrasive cutting resistances, but would poorly perform at impact tests. A high hardness is essential for a high abrasive resistance but, hardness and ductility are two contrary properties. Due to the contradictory characteristics of required properties, only composite materials of carefully chosen material combination can adequately resist burglary attacks. Therefore, good performing materials from the previous tests are chosen and in selected combinations, the materials together can produce an overall good performing composite material. Three different composite materials will be proposed in the following chapters. The performances are compared to steel as well as the prices of the used materials. The production costs will be neglected.

Furthermore, suggestions for improvements and process optimizations are given for the developed composites.

9.1 Steel, Copper and, Ceramic Composite

The three materials steel, copper and silicon nitride have been chosen due to their excellent single performances in the previous three chapters. The ceramic silicon nitride has proven its abrasion resistance in chapter 6. Copper showed the best resistance against thermal cutting since at adequate thicknesses not cutting through has been found. Steel is chosen to give the composite its required impact resistance.

9.1.1 Structure of the Composite

Silicon nitride has a good availability due to its use in the chipping production in form of tool inserts. Here it is used because of its abrasive resistant nature. Silicon nitride inserts with a diameter of 9.525 mm and a thickness of 3.175 mm (ANSI: RNGN-32, Grade: GSN100, Manufacturer: Greenleaf Corporation) are used in the composite. Tests in chapter 6 proposed that the full potential of silicon nitride can be developed if it is embedded in a matrix. Therefore, the round inserts are pressed into equally sized holes that are drilled into the 6.3 mm thick steel plate. The holes are 20 mm apart from each other. The steel is a high strength low alloy steel 5160 with a yield strength of 670 MPa (Supplier: McMaster-Carr, Steel meets ASTM A689) and was proven to resist the specified impact energies. A 110 copper plate (meets ASTM B137, Supplier: McMaster-Carr) encloses the inserts into the composite. Figure 22 shows the schematic of the composite.

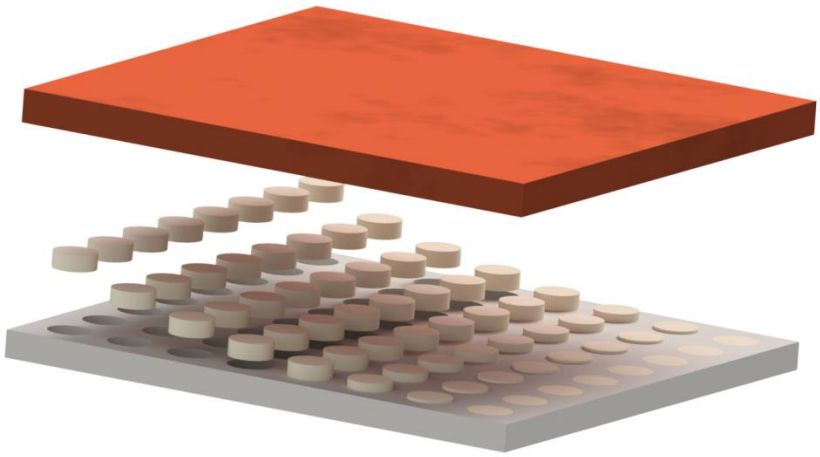

Figure 22: Steel ensures the impact strength as well as the best performance of the silicon nitride inserts. The copper plate encloses the inserts into the sandwich structure.

The copper plate and steel plate are than bonded in a brazing process. The brazing process is chosen because of the easy joining of large plates without distortion due to thermal stresses. Additionally, copper and steel can be joined easily in a brazing process which is not the case for traditional arc welding processes since the high effusivity of copper hinders the process. A 0.12 mm thick silver braze (45 % Ag, 30 % Cu, 25 % Zn, Manufacturer: The Prince & Izant Company) with a recommended brazing temperature of about 780 °C is used to join the plates (argon atmosphere required). The strength of the brazing joint is technically able to surpass the yield strength of copper, which ensures a sufficient bonding. The different thermal expansion coefficient of steel and copper cause stresses in the brazing joint, which have to be verified in order to ensure adequate bonding. The stresses occur during the cooling phase from solidification of the brazing alloy at 660 °C to room temperature. Figure 23 shows the remaining stresses at room temperature. A 450 mm x 450 mm safe wall

serves as the simulation model. Symmetry is used to reduce the calculation expense. The maximum occurring stresses of 112 MPa can be accommodated by the joint. The used parameters for the simulation are selected from the engineering data source of Ansys. The decisive parameters are:

- Thermal expansion coefficient steel: $1.12*10^{-5}\ K^{-1}$
- Thermal expansion coefficient copper: $1.8*10^{-5}\ K^{-1}$
- Young's modulus steel: 210000 MPa
- Young's modulus copper: 110000 MPa

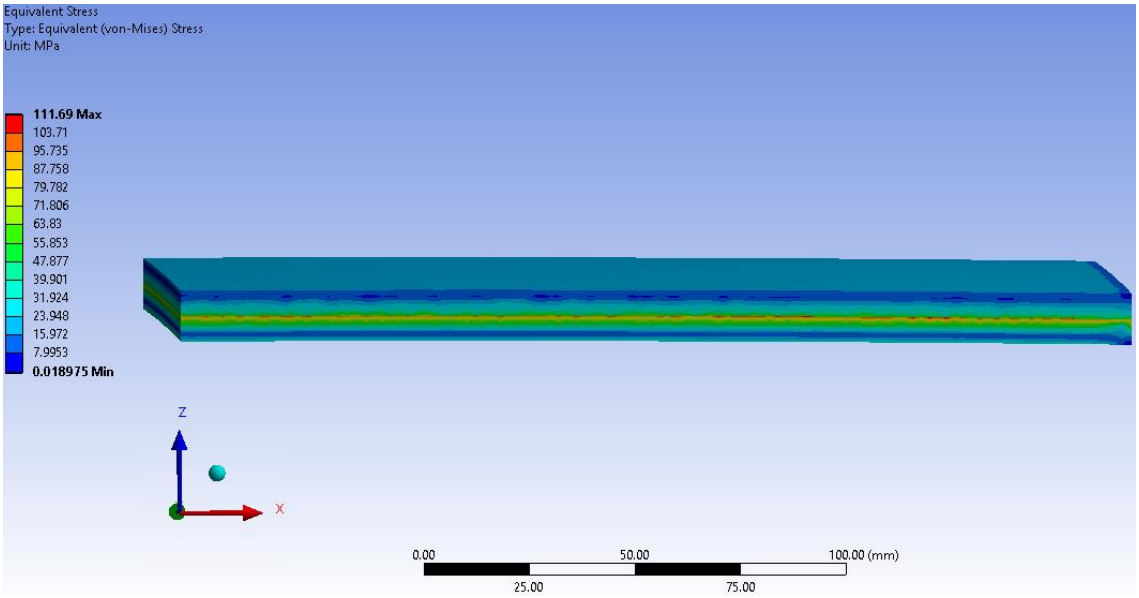

Figure 23: Stresses in the composite after cooling from 660 °C to 20 °C. The highest stresses occur in the brazing zone, between the copper and the steel, indicated by the red colored zone.

The necessary thickness of the copper plate is dependent on the time it has to resist the thermal cutting, as well as the power of the thermal cutting device. The dimensioning will be discussed in the following paragraph.

9.1.2 Dimensioning of the Copper

Results from chapter 7 proved that a 6.3 mm thick 110 copper plate can resist the exothermic cutting lance for more than 34 seconds without damage. However, the copper of a limited size serves as a heat storage, and as soon as the copper reaches temperatures around the autoignition temperature or the melting point the copper will fail similar to an ATM safe made of steel. Therefore, the right dimensioning in size and thickness of the built-in copper is necessary. A computer model (Software: Ansys Workbench 2017) is helpful to enable the dimensioning dependent on the required resistance time, size of the safe and power output of the thermal lance. To develop this model, practical exothermic cutting tests are performed on copper and the results are than true to the original reproduced in the computer simulations. The practical copper test samples are equipped with three thermocouples with a defined distance to the point where the thermal lance tries to penetrate the copper. The sketch in figure 24 shows the positions of the thermocouples and the point of penetration. A copper plate with the dimensions of 302.5 mm x 101.5 mm x 6.3 mm is used in the test.

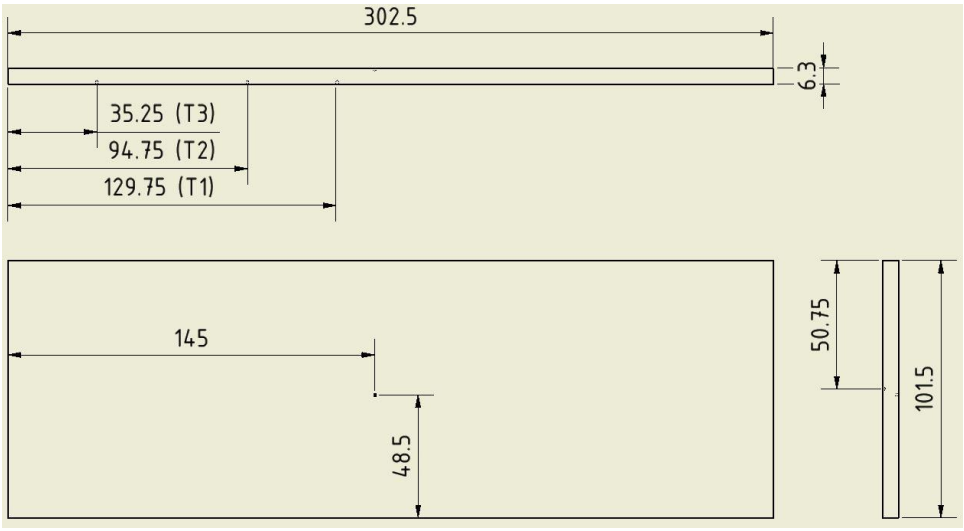

Figure 24: Sketch of the copper sheet used for the measurements. The point where the thermal lance penetrates the sample is indicated, as well as the positions of the three thermocouples (T1, T2, T3) from the other side of the sheet. Dimensions in millimeter.

During the tests the power output of the thermal lance transferred to the copper is of the range between 4500 J/s and 4800 J/s and is dependent of the functioning of the operating person. The temperature profile of the practical test is presented in figure 25, as well as a picture of the thermocouple attachment and a picture of the attacked point. Additional information and simplifications for the computer model can be gained from the practical model besides the temperature profile. A crater with a diameter of 10 mm and a depth of 1 mm formed in the middle of the attacking point. The temperatures must have reached the autoignition temperature (1065 °C) or the melting temperature (1085 °C) [42]. This area is exposed to the highest power. Around the attacking point with a diameter of 30 mm, a second area occurs in which power of the thermal lance is transmitted to the copper as well. Outside of this 30 mm diameter the combustion products

(oxides) condensate on the colder copper, build up and lead away the hot jet from the copper.

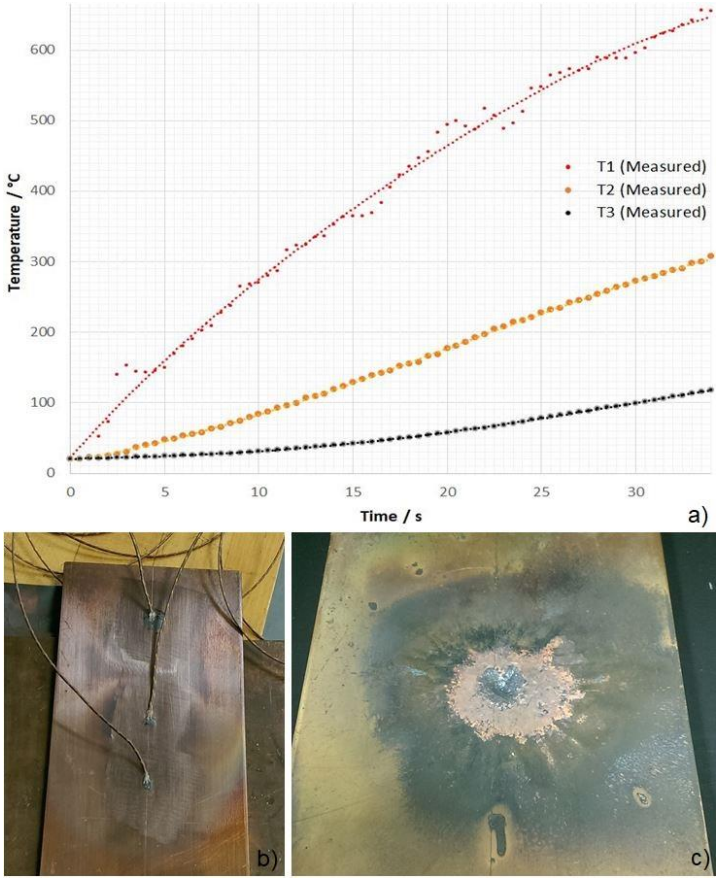

Figure 25: The diagram a) shows the temperature profiles of the measured temperatures T1, T2, and T3. The thermocouples are welded to the copper plate to ensure a proper heat transfer shown in picture b). Picture c) demonstrates the crater caused by the thermal lance. Three different areas can be determined; the crater, a copper colored circle around the crater about 30 mm in diameter, and a darker area where the oxides condensed (oxides removed for picture).

In the simulation model, the assumption of zero heat transfer is made in this area of condensation and also further out. This means the power output of 4800 J/s (highest value chosen) is split into two areas of heat transfer in the computer model, but the distribution has to be defined. The energy distribution between

these two areas is predicted and then adjusted until the theoretical temperature profile matches the practical temperature profile. In Figure 26, the theoretical and practical model are compared.

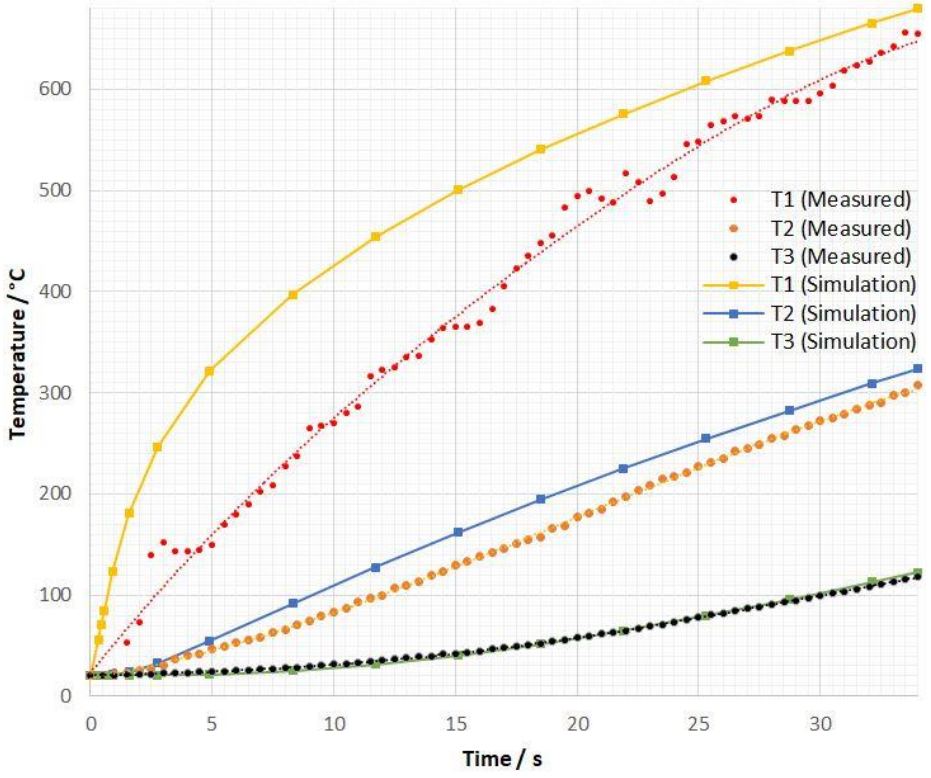

Figure 26: Temperature profile comparison of the simulated model and the practical measured copper sheet.

The temperature profiles of T3 are in very good agreement for both models, but the temperature profiles for T1 and T2 show partially strong deviations even though the same amount of energy is introduced into both models. The deviation for the practical model, which always shows a lower temperature than the simulation model, can be explained by the fact that the heat exchange between the thermocouples and the copper is not perfect as it is assumed in the simulation model. Therefore, deviations increase where the heat exchange is

more pronounced. T3 shows the biggest deviation followed by T2 and then T3 with insignificant deviations.

The used parameters for the simulations are as follows:

- Density: 8960 kg/m^3
- Isotropic thermal conductivity: 390 W/(m*K)
- Specific heat: 385 J/(kg*K)

Additionally, the copper plate is exposed to radiation and convection loses to the atmosphere (20.8 °C) with a emissivity of 0.04 and a convection of $1*10^{-5}$ W/(mm^2 * K). The 30 mm diameter attacking point is exposed to radiation from the 3000 °C thermal lance (emissivity: 0.04). Further the crater of 10 mm in diameter receives a convection of 0.0197 W/(mm^2 * K) against the 3000 °C of the thermal lance. The rest area of the attacking point receives a convection of $9.8*10^{-4}$ W/(mm^2 * K) against the 3000 °C of the thermal lance.

With these parameters, copper sheets for the construction of safes can be constructed in every arbitrary size for the required resistance time. For example, the copper plate of 302.5 mm x 101.5 mm used for the practical test would still resist the exothermic cutting attack at a thickness of 6 mm for 34 seconds according to the simulations. Practical tests could confirm this result.

It is also mentionable that the thickness of a cooper sheet can be significantly reduced if the copper is cooled with water from the backside during the attack. Copper thicknesses of 1.5 mm cooled by water showed sufficient resistance in tests. The high specific energy and the high energy of vaporization of water make

the required heat dissipation possible. Solutions with hydrogels were tested, but due to construction and corrosion challenges, these solutions were not further investigated.

9.1.3 Performance and Costs

The composite was tested similarly to the performed tests in chapter 6, 7 and 8. The exothermic cutting could not penetrate the copper sheet. The thermal cutting was tested from both sides to determine if the cutting from the steel side could increase the heat exposure due to additional provided fuel through the burning steel sheet. Both tests could not penetrate the copper. However, the cutting from the steel side destroyed the steel sheet with a radius of 15 mm around the attacking point (figure 27).

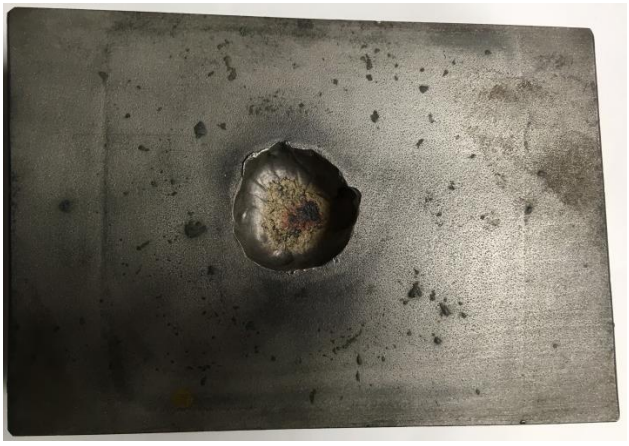

Figure 27: Crater in the composite material after attacking it from the steel side with the exothermic cutting lance. The thermal lance could penetrate a 30 mm wide crater in the steel, but could not penetrate the copper.

Additionally, the thermal cutting with high and low oxygen pressure could also not penetrate the copper sheet. Merely a deeper crater was produced during the

cutting with lower oxygen pressure, indicating the higher power output during cutting.

Impact tests with the drop tower confirmed the previous tests that the high strength steel cannot be extensively deformed with the impact energy of 53 J. The high ductility of copper could further improve the impact performance. Nevertheless, a small stripe of the composite was deformed in the impact test to examine the brazing connection between the steel and copper. After the deformation the braze was intact as figure 28 demonstrates.

Figure 28: Picture a) shows the deformed composite stripe. In picture b) the brazing joint of the most deformed middle part is examined.

The abrasive cutting results are cumulated in figure 29 a) and b). The embedded silicon nitrides caused a high wear to the cutting blade, which was mentioned in chapter 6, too. The poor abrasive cutting resistance of copper influences the whole performance of the composite by raising the removed volume per time to an average level of good performing steel of equal thickness.

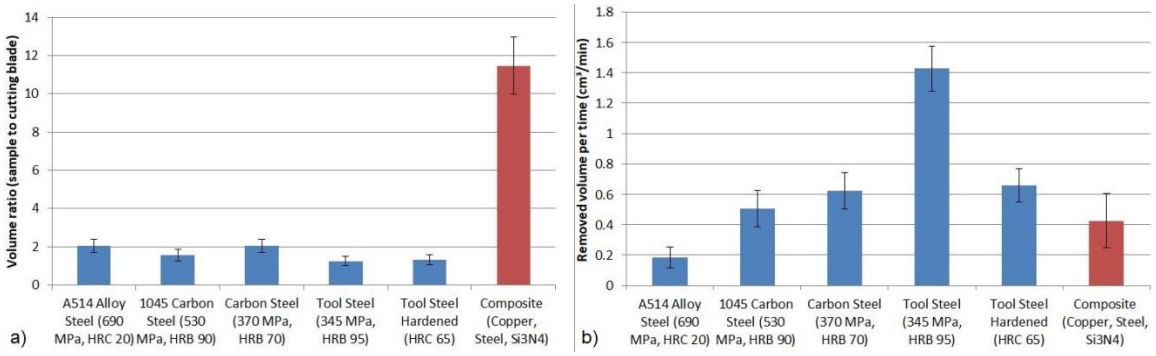

Figure 29: Abrasive cutting performance of the composite material (red), compared to common steels. Diagram a) shows the volume ratio performance and diagram, b) shows the removed volume per time, again compared to common steels.

In terms of the price, the composite material is 5 to 6 times more expensive than equally thick high strength steel. The price is about $29,500 to $37,111 for a cubic meter of the composite material, whereas the price of high strength steel is about $5,300 to $6,400 for a cubic meter [36]. Copper makes up the largest fraction of the price with 71-75%, followed by 16-20% for the silicon nitride and 7-8% for the steel. Process costs and time are not taken into account. The impact resistance is as well poorer for the composite than for equally thick high strength steel. The thermal cutting resistance is significantly increased.

9.1.4 Suggestions for Improvement

The abrasive resistance can be increased by decreasing the distance between the silicon nitride inserts, which would increase the number of inserts per area. However, this measure increases the cost and decreases the impact resistance of the composite due to a weakened steel sheet. The holes in which the inserts are pressed influence the impact resistance negatively because they reduce the transverse section of the steel as well as the notch effect can favor crack

initiation. The drill holes should have rounded edges, which can be produced with rounded-edge end mills. Furthermore, the arrangement of the inserts has to be chosen so that during the immersion of the cutting blade, an insert is always hit. Additional improvements have to face the costly and time consuming brazing technology. This is problematic due to the high thermal and electrical conductivity of the copper, conventional resistant welding processes cannot be used for the fast joining between the copper and the steel. Cold pressure welding, with or without intermediate layer, and resistance welding with intermediate layer could be an alternative to the time consuming brazing process.

9.2 Resin, Fiber, and Boron Carbide Composite

Similar to the previous presented composite, this composite contains also three different materials. Each material of these materials exhibits excellent resistances in one of the three common attack categories. Boron carbide is used to resist the abrasive cutting, phenolic resin is used to resist the thermal attacks, and the fibers can resist impacts due to their high strength. The detailed structure and the performance will be discussed in the following paragraphs.

9.2.1 Structure of the Composite

Boron carbide has one of the highest H/E ratios among all materials as presented in chapter 6. On the other hand, it has a poor fracture toughness but as previously discussed the fracture sensitivity decreases with decreasing size. Therefore, boron carbide is used in form of small particles with a mesh size of 5-60 (Supplier: Feldco International). However, the particles have to be embedded into a matrix as a supporting structure. Here, a phenolic resin (ground phenol-

formaldehyde novolac containing hexamethylenetetramine, Supplier: Plastics Engineering Company) is used that is characterized by a high thermal cutting resistance. Phenolic resin is very brittle and sensitive to fracture, which makes it by definition a weak impact resistant material. To increase the impact performance, high strength fibers are additionally embedded into the phenolic resin. The high strength fibers ensure an adequate tensile strength, as well as an increased elasticity. Fibers of the Japanese company Toyobo are chosen due to the high tensile strength of 5800 MPa and an elongation at break of 3.5 %. These fibers surpass the mechanical properties of the well-known aramid fibers (Kevlar). All three components were joined in a hot-press casting process at a temperature of 140 °C for 15 minutes with a pressure of about 6.5 N/mm^2. Afterwards, the composite rests for one hour at 100 °C. Before the hot-press casting process, the raw materials were prepared as follows:

1. The bottom of the casting mold was coated with phenolic resin with 7.5 wt.% fibers until the bottom was covered.
2. A woven fabric of the fiber was laid on top. The woven fabric was wetted with a phenol-formaldehyde resol in aqueous solution before. (Supplier: Plastics Engineering Company)
3. Then the boron carbide particles, in combination with phenolic resin with 7.5 wt.%, were added. Also, the boron carbide particles were wetted with the aqueous resin before.
4. A woven fabric wetted with the aqueous resin covered this layer.
5. On top, a covering layer of phenolic resin with 7.5 wt.% fibers was added.

6. The negative casting mold was attached.

In total, about 19 g of aqueous resin, 2 g of woven fabric, 38.5 g of boron carbide, and 54 g of phenolic resin with 7.5 wt.% was used to produce a composite sample. Two woven fabrics were added to relieve the outer surfaces where the highest stresses occur during bending or impacts. The woven fabrics and boron carbide particles are wetted with the aqueous resin to increase the mechanical bonding with the matrix. In figure 30 a prepared composite sample is demonstrated.

Figure 30: Composite material after the casting. The demonstrated sample has the dimensions of 98 x 75.5 x 7.5 mm.

9.2.2 Performance and Costs

At first, the abrasive cutting performance is measured depending on the boron carbide particle size to define which particle size is favored for a high abrasive resistance. Composite materials are produced with the same weight of boron carbide with the mesh size of 5, 7-12, 20, and 60. In figure 31, the results are compared to each other. It can be seen that with an increasing particle size, the

abrasion resistant changes to more favorable values. The maximum is reached with a boron carbide particle size of 5 mesh (4 mm). The better performance of the composite with increasing particle size can be explained by the “softening point” of the phenolic resin. The occurring high temperatures during the abrasive cutting lead to a softening of the phenolic resin matrix, which weakens the bonding between the particles and the matrix. Small particles were found to break away from the matrix during the cutting, but with increasing particle size the detaching from the matrix is impeded. The bigger particles have to be severed by the cutting blade, whereas small particles detach from the matrix.

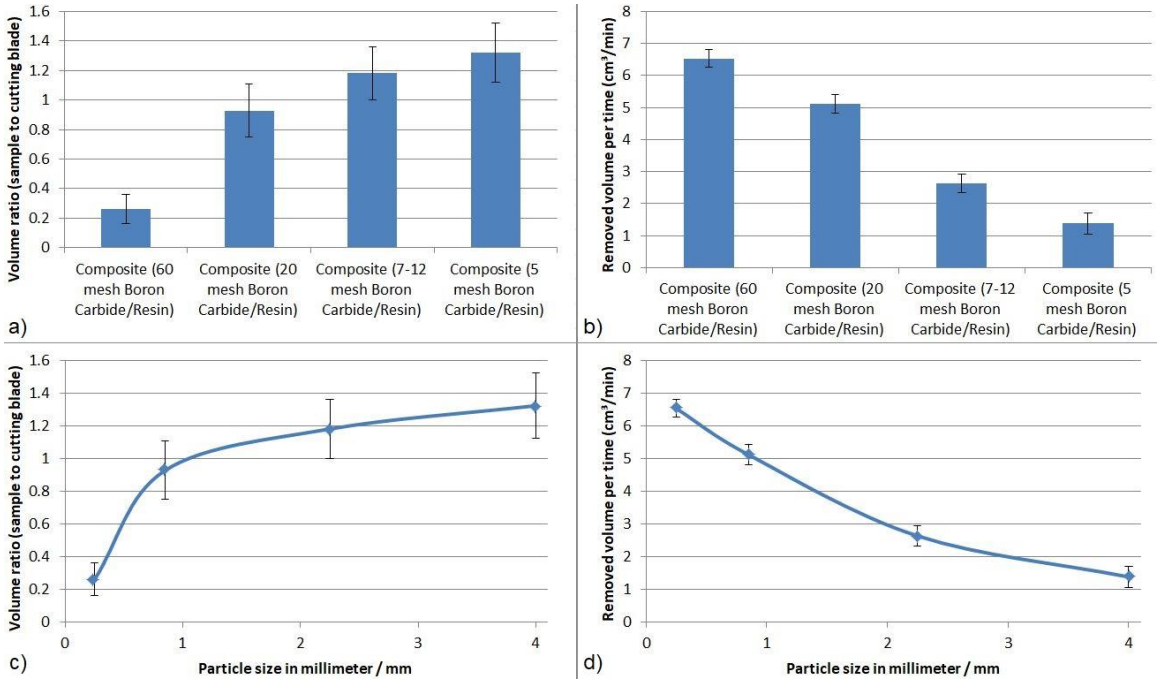

Figure 31: Comparison of the composites with different particle sizes. In diagram a) and c) the volume ratio is compared, whereas diagram c) gives a better estimation of the volume ratio due to a continuous x axis. In the diagrams b) and c) the removed volume per time is compared and again in diagram d) a better estimate can be made of the values. The diagrams c) and d) also indicate that the resistant values stagnate with further increasing particle sizes.

The best performing composite is compared with steel. The composite with the 5 mesh boron carbides shows sufficient resistance values and is able to surpass the abrasive resistance of some low strength steels. In figure 32 the common steels are compared to the composite.

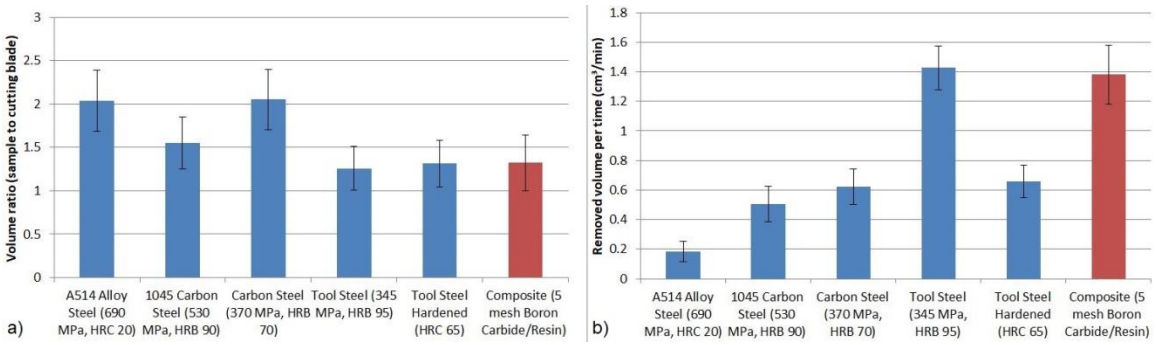

Figure 32: Volume ratio of the abrasive wear a) and the removed volume per time b).

The composite material is also compared to steel in terms of the thermal cutting resistance. The tests show that the composite surpasses the thermal cutting resistance of steel by far. Composite thicknesses smaller than 5 mm have an equal cutting resistance to steel with a thickness of 25.4°mm, which would fulfill the requirements of the standards. However, the composite cannot compete with the impact strength of steel. In the drop tower test, the composite with a thickness of 8.5 mm could just absorb the energies of 5 impacts, whereas steel can absorb many more impacts as mentioned before. One weakness next to the brittle nature of the phenolic resin is that the mechanical bonding between the matrix and the fibers is not sufficient and is destroyed during the impacts. Figure 33 demonstrates the destroyed composite material.

Figure 33: Composite after the drop tower test. Six impacts were needed to penetrate the material with a thickness of 8.5 mm.

To have a better measurement of the impact resistance, the flexural strength is measured in a three point bending test. The three point bending test gives a measure of the maximum flexural strength, the elasticity/plasticity and therefore an estimation of the impact resistance of the composite. Commonly, brittle materials such as concrete are measured with this procedure. Figure 34 shows the results of the bending test for two tested samples.

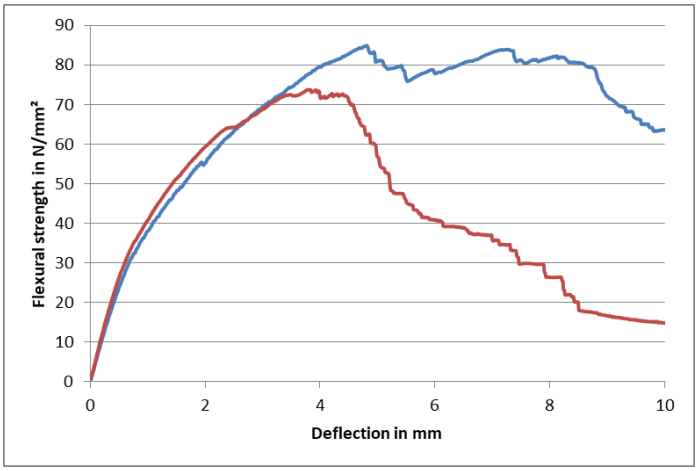

Figure 34: Flexural strength over the deflection in the middle of the composite plate. The supports were 80 mm apart from each other. The blue curve was a sample with the width of 61.8 mm and a thickness of 7.16 mm. Red curve 59.5 mm to 6.94 mm.

The two curved shapes develop differently at the deflection of 4 mm, which is due to the inhomogeneous distribution of the woven fabric as well as the boron carbide particles that can introduce fracture with their sharp edges. Nevertheless, flexural strength of 70 MPa to 85 MPa were reached by the composites which can compete with the flexural strength of concrete (30 to 85 MPa) [71]. The main disadvantage of this composite is the lack of deformability, but former studies on phenolic resins showed that the elasticity can be increased by the addition of polyvinyl butyral [72]. Four samples were prepared to prove this statement. Two samples with phenolic resin and 7.5 wt.% fibers. The other two with phenolic resin 10 wt.% polyvinyl butyral and 7.5 wt.% fibers. The addition of woven fabric and boron carbide particles was renounced to maintain a more homogeneous composite. In figure 35 the results of the three point bending test are cumulated.

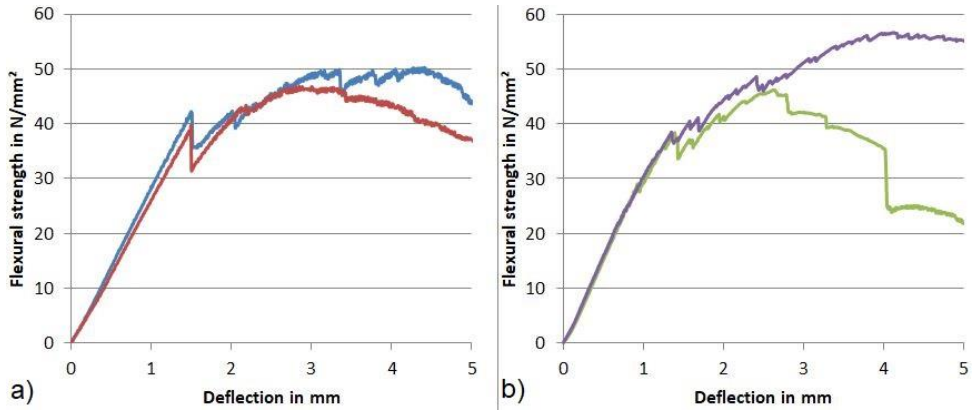

Figure 35: Diagram a) shows the two composites without polyvinyl butyral. The blue line indicates a sample with the width and thickness of 35.7 mm and 4.44 mm. Red line 38.12 mm and 4.34 mm. Diagram b) shows the two composites with polyvinyl butyral. The violet line indicates a sample with the width and thickness of 37.2 mm and 6.24 mm. Green line 36.6 mm and 6.15 mm. The supports were 80 mm apart from each other.

The Young's modulus of the composites without polyvinyl butyral is about 6400-6700 MPa, whereas the Young's modulus is about 5300-5400 MPa for the samples with polyvinyl butyral. Significant differences between the flexural strength cannot be seen among the four samples. The maximum flexural strength is between 45 MPa and 55 MPa for all samples. A reduced Young's modulus by an equal flexural strength indicates an increase in the elasticity for the samples treated with polyvinyl butyral.

One of the main advantages of the phenolic resin, fiber, and boron carbide composite is that it has a density of about 1.6 Kg/dm^3, which is almost five times lighter as steel. Cost wise, it seems to have an advantage over steel since the main component phenolic resin is just half the price of steel by volume. However, the price of phenolic resin increases by a factor of 20 with reinforcement. The boron carbide with 35 wt.% produces the highest costs of the composite making it 14 to 17 times more expensive than steel. The cost per cubic meter composite is about \$76000-\$114000 [36]. On the other hand, one fifth of the composite material is needed to have an equal thermal cutting resistance to steel, which makes the composite three times more expensive than steel in terms of the thermal resistance.

9.2.3 Suggestions for Improvements

Aside from the good, light weight, and thermal cutting performance of the composite, further potentials can be easily developed. One improvement has to address the softening point of the phenolic resin. Then, with an increased softening point, the mechanical bonding between the abrasive particles and the

matrix can be increased at elevated temperatures. That means less particles would break off and more particles have to be severed by the cutting blade. This improvement can reduce the fraction of boron carbide needed which makes more matrix material available to resist impacts and reduces the costs. Additionally, the impact resistance has to be increased further. Polyvinyl butyral is just one solution. Different reinforcing fibers can be examined according to their mechanical and chemical bonds to the phenolic resin. Fibers might be available with lower strength but increased bonding to the resin, which favors the impact resistance. Furthermore, different abrasive particles can improve the cost. Coarse grained bauxite was used during the abrasive cutting tests but did not reach the performance of equally sized boron carbide. Fine grained zirconium carbide and aluminum oxide (80 mesh) also could not produce adequate results, but coarse grained aluminum oxide and zirconium carbide could be an alternative to the boron carbide. So far, fragmented boron carbide served for the particles in the composite, but fragments are always identified with sharp edges which favor the initiation of cracks in the composite. Improvements could address this, too.

9.3 Cemented Tungsten Carbide and Steel Composite

Hard tungsten carbides embedded into a cobalt matrix showed outstanding performances in the abrasive and thermal cutting tests. A cobalt matrix is necessary to counteract the brittle nature of the tungsten carbides. However, the impact evaluation in chapter 8 predicts that the impact resistance is not as pronounced as steel. Therefore, the cemented tungsten carbide sheets can be

equipped with steel to enhance the impact performance. The cobalt content can also affect the impact resistance.

9.3.1 Structure of the Composite

The used cemented tungsten carbides consist of 1.4-2.0 µm tungsten carbides particles and cobalt as the matrix. The tungsten carbides and cobalt are joined in a sintering process to produce a dense and homogeneous structure. The hard and thermally staple tungsten carbide particles are associated with the good abrasive and thermal cutting performance of the composite. The cobalt gives the composite its toughness and with increasing amounts of cobalt, the toughness is enhanced, but the cobalt content affects the other two properties, too. To examine the influence, four different tungsten carbides with different amounts of cobalt are examined (Supplier: Zhuzhou Tongda Carbide Co., LTD):

- Tungsten carbide with 6 wt.% cobalt, Hardness 1500 HV, Flexural strength: 1800 MPa, Thickness 6.5 mm
- Tungsten carbide with 10 wt.% cobalt, Hardness 1300 HV, Flexural strength: 1900 MPa, Thickness 6.5 mm
- Tungsten carbide with 15 wt.% cobalt, Hardness 1020 HV, Flexural strength: 2100 MPa, Thickness 6.5 mm
- Tungsten carbide with 20 wt.% cobalt, Hardness 820 HV, Flexural strength: 2500 MPa, Thickness 6.5 mm

The microstructure of each composite is presented in figure 36.

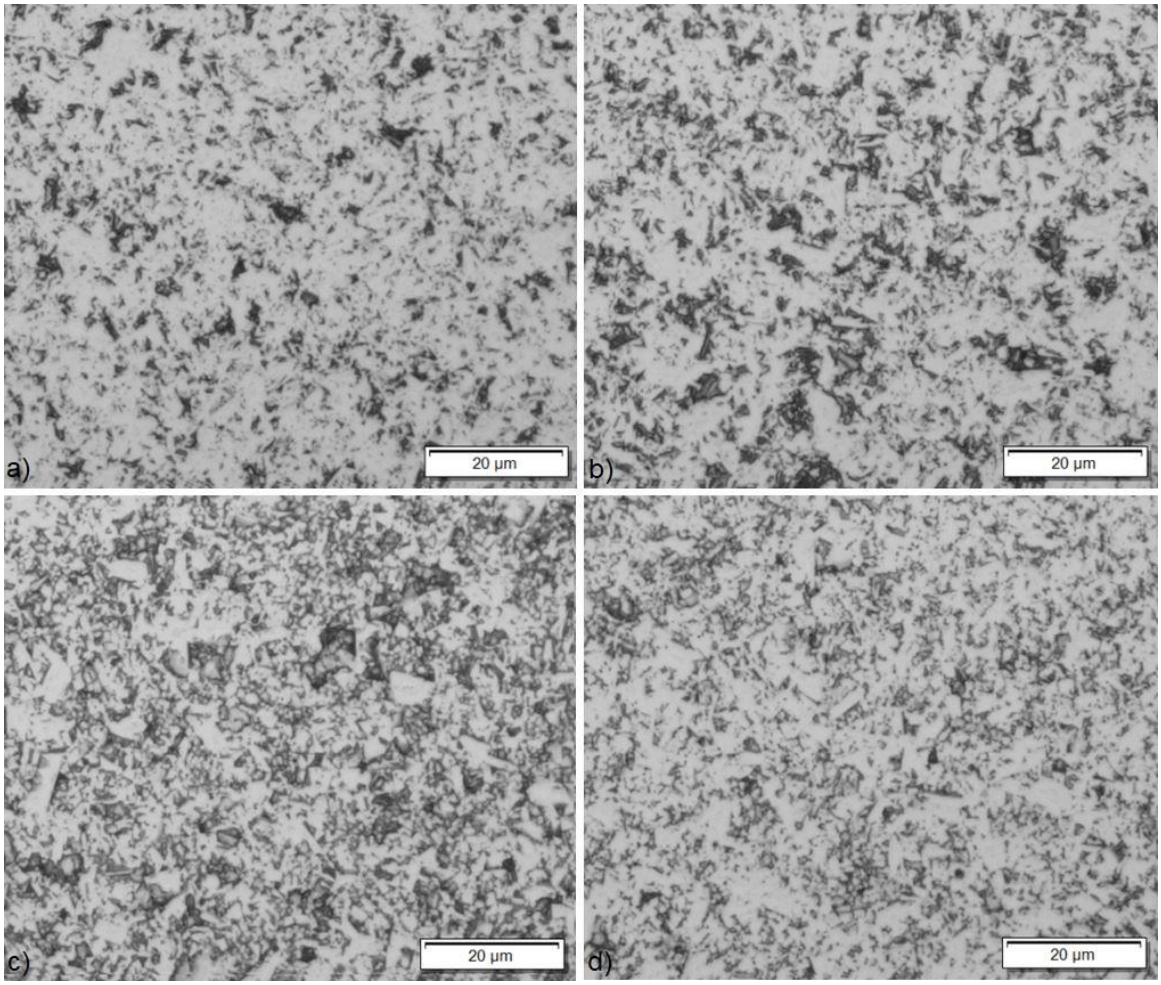

Figure 36: Microstructure of the cemented tungsten carbides. Cobalt content increases from 6, 10, 15, to 20 wt.% from picture a) to d). The tungsten carbides appear brighter whereas cobalt appears darker.

Low fracture toughness and a poor ductile behavior make the cemented tungsten carbides sensitive to impacts. Also, here the cemented tungsten carbide sheets can be sandwiched into two high strength steel sheets (Yield strength: 690 MPa, Thickness: 1.57 mm) that are brazed to the composite. A silverbraze with 49 wt.% silver, 16 wt.%, 23 wt.% zinc, 7.5 wt.% manganese, and 4.5 wt.% nickel is used (Supplier: The Prince & Izant Company). The brazing temperature is

750 °C. Occurring stresses due to different thermal expansion coefficients are simulated with Ansys (see figure 37).

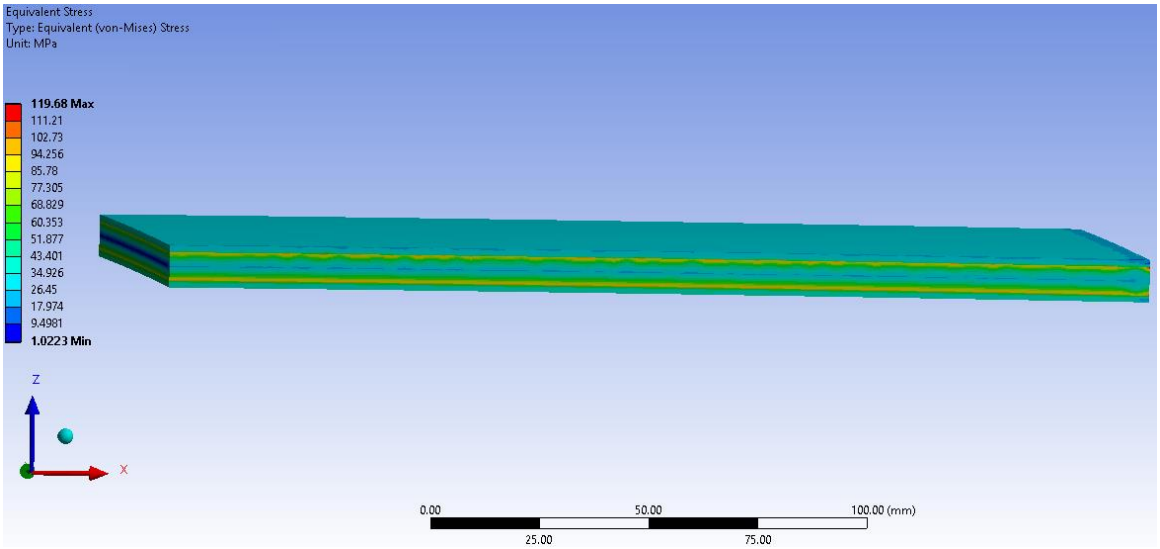

Figure 37: Occurring stresses during the cooling from 660 °C (solidification) to room temperature for a 450 mm large wall (symmetry used). The highest stresses appear in the two brazing joints. Used material parameters for steel are Young's modulus 210000 MPa and thermal expansion coefficient $1.2*10^{-5}$ K^{-1}. Cemented tungsten carbide 20 wt.% cobalt: Young's modulus 500000 MPa and thermal expansion coefficient $6.4*10^{-6}$ K^{-1}.

9.3.2 Performance and Costs

In chapter 6 the outstanding abrasive cutting resistance was pointed out. The removed volume per time was more than 10 times lower than for the best performing steel. Additionally, abrasive cutting tests with the cemented tungsten carbides showed that the abrasive resistance decreases with increasing cobalt content. In figure 38 the abrasive cutting resistance is plotted over the cobalt content.

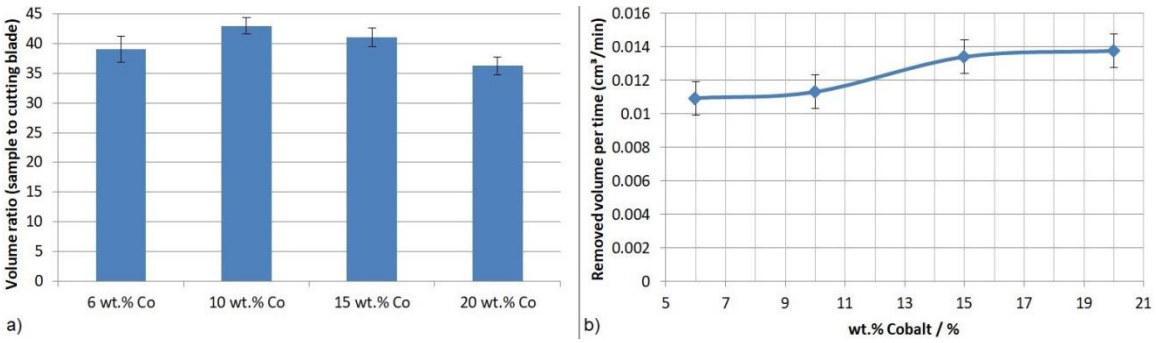

Figure 38: Volume ratio of the abrasive wear a) and the removed volume per time b) for cemented tungsten carbides with different cobalt contents.

With increasing cobalt content, less of the hard tungsten carbides resist the cutting. The decreasing hardness is also an indicator for the regressing abrasive cutting resistance but compared to steel stays on a very high level.

Similar results are found for the thermal cutting resistance. With increasing amount of cobalt, the thermal cutting resistance decreases indicated by an increasing cutting speed with cobalt content (see figure 39). This behavior is different from other oxidative studies on cemented tungsten carbides where the oxidation resistance increases with cobalt due to the formation of protective oxide layers [55][57]. However, in these studies the melting point of cobalt was not exceeded. The four cemented tungsten carbides were also tested with the drop tower test to analyze the impact resistance. The flexural strengths of the composites predict increases in the impact resistance with increasing cobalt content. The composites with 6, 10, and 15 wt.% cobalt could not resist the impacts whereas the 20 wt%. cobalt composite could resist the impacts.

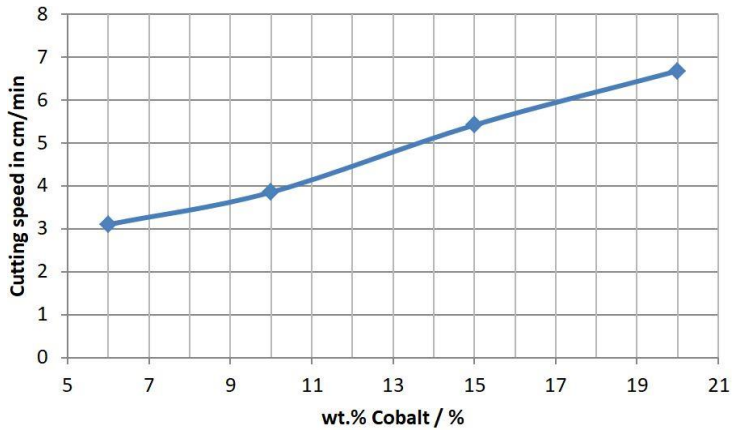

Figure 39: Exothermic cutting speed for cemented tungsten carbides with different cobalt contents. The thickness of the samples was 6.5 mm.

As a measurement of the absorbed energy, an acceleration sensor was used during the impact test to visualize the impact performance. The results are cumulated in figure 40. A fast furrier transformation is used to allow a more meaningful comparison. A small fraction of the acceleration waveform is the actual deceleration of the hammer, indicated by a small amplitude with a wider width at the beginning. The rest of the waveform is the high frequency vibration of the hammer parts. The small amplitude with a wider width at the beginning is narrower for samples that broke during the impact which signals a shorter impact. The cemented tungsten carbide with 20 wt.% produced a wider amplitude due to the longer impact and reflection of the hammer. Therefore, in the fast fourier transformation, the peak at low frequencies represents the impact and the rest of the frequencies represent the vibration of the hammer. The height of the aptitude at low frequencies increases with increasing cobalt content, which indicates the increased energy dissipation.

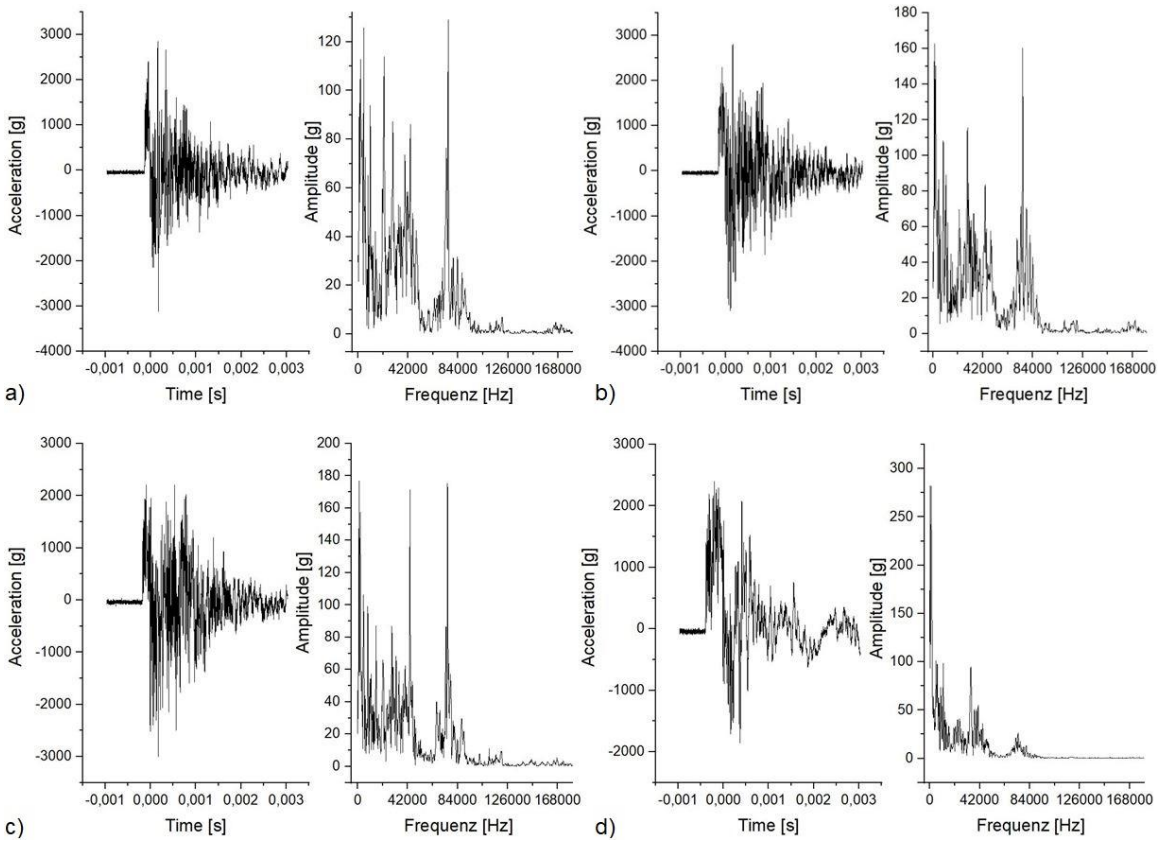

Figure 40: The pictures a) to d) show the trop tower results for cemented tungsten carbides with 6, 10, 15 and 20 wt.% cobalt. The left diagram demonstrates the acceleration measured and the right diagram demonstrates the fast furrier transformation.

Cemented tungsten carbide with 6 wt.% was equipped with 1.57 mm thick high strength steel (Yield strength: 690 MPa) sheets from both sides in a brazing process. This composite could not be destroyed/deformed with the drop tower test.

The costs of cemented tungsten carbide are 150 to 200 times more expensive than steel volumetric wise. The price decreases with increasing cobalt content from about $1,500,000 per cubic meter for a composite with 6 wt.% cobalt, to about $1,250,000 per cubic meter for a composite with 20 wt.% cobalt [36].

However, dependent on the steel used, the removed volume per time is 10-100 times lower for the cemented tungsten carbide.

9.3.3 Suggestions for Improvement

Cemented tungsten carbide with 20 wt.% cobalt could pass the drop tower test, but has as demonstrated in chapter 8 poor fracture toughness's. Small surface defects or notches in the ATM safe construction could cause the failure of this material. Improvements have to address the toughness and ductility of the material with a view to the thermal and abrasive cutting resistance. A further increase in the cobalt content could increase the toughness by reducing the price. Nevertheless, this would reduce the thermal and abrasive resistance. Research studies on tungsten carbide/cobalt particles embedded in a mainly iron matrix have been published [73]. These composites could decease the costs and increase the toughness, but the effect on the other properties has to be observed. Another way could be to bond with steel as proposed. Resistance welding processes with a nickel intermediate layer could improve the joining process.

10 Conclusion

The aim of this research was it to find and develop new materials for secure storage systems. The selection of the material took place on the basis of the fulfilment of the common European and American standards, EN 1143-1 and UL 291. This would guarantee the certification of the developed materials. For the selection of potential safe materials, individual test procedures were devised to find the best materials in the most common burglary attack categories: Abrasive resistance, thermal resistance, and impact resistance. With a constructed abrasive cutting device, it was possible to evaluate several materials for their abrasive resistance. The scientific background, by means of newest publications, is explained for the found abrasive resistance. In general, materials with a high hardness, pronounced hardness to Young's modulus ratio, and adequate thermal shock resistance showed the best results; silicon nitride and cemented tungsten carbide, to name a few. To examine the thermal resistance, an exothermic cutting procedure is chosen. Materials with a generally high oxidation resistance also showed good performances in the thermal cutting tests. For example, stainless steel performed better than steel, and steel performed better than aluminum with poor oxidation stability. However, the effects of resistance vary between materials groups and also in material groups. The scientific reasons for a good performance were pointed out. Copper, graphite, phenolic resins, and cemented tungsten carbides showed excellent resistance over steel. The impact

resistance is evaluated with theoretical, computer simulation attempts, as well as drop tower tests. The results shows that materials with a high ductility and high strength achieved by steels, alloy steels, and nickel alloys have the best impact resistances. An average, good performing material in all three categories was proposed to be a safe material, but due to the strong differences in the properties a single good performing material did not exist. Therefore, three composite materials were introduced that fulfill the standards and perform equally or better than steel in at least two of the burglary attack categories. A copper, steel, silicon nitride composite and a phenolic resin, fiber, boron carbide as a promising low weight composite, as well as a cemented tungsten carbide steel composite were introduced. The development of the composites pointed out that with the enhancement of a resistance category, at least one of the other resistance categories is negatively influenced. This behavior is called Pareto efficiency and becomes more pronounced in consideration of the costs. An important factor during the development of composites is also that these are as homogeneous as possible, which would favor the overall performance. The small tungsten carbide particles (1.4-2.0 µm) embedded into a cobalt matrix is an example for a homogenous composite. A solution to improve the commonly used steel in safes could also be the use of TRIP-Steels and TRIPLEX-Steels that can maintain the impact resistance, improve the abrasive resistance due to hard precipitations, slightly increase the thermal cutting resistance due to the alloying elements which increase the oxidation resistance. Future improvements have to address the light weight phenolic resin composite as well as the attempt to use cemented tungsten

carbides. Sintering processes might be able to process other hard and cheaper carbides in a more ductile matrix such as iron.

Bibliography

[1] Secure storage units – Requirements, classification and methods of test for resistance to burglary – Part 1: Safes, ATM safes, strongroom doors and strongrooms; EN 1143-1:2012

[2] Standard for Automated Teller Systems; UL 291 February 15, 2012

[3] Agreement on Safes and Strongrooms; European Fire and Security Group; MA Safes - Version 7 October 2016

[4] Information about the ESSA and European Certification Body; (www.ecb-s.com/_rubric/index.php?rubric=ESSA+EN+Press+Infos-zu-ESSA)

[5] ATM Benchmarking Study 2016 and Industrial Report; (www.accenture.com/_acnmedia/PDF-10/Accenture-Banking-ATM-Benchmarking-2016.pdf)

[6] The European ATM Security Team: European ATM Crime Report 2014, Version 1.1, April 2015 (www.european-atm-security.eu)

[7] European Association for Secure Transactions: ATM Crime Report, (www.association-secure-transactions.eu/tag/atm-crime-report/)

[8] ATM Industry Association (ATMIA): Best Practices for Preventing ATM Gas and Explosive Attacks 2014, (www.atmia.com)

[9] Fumanelli, G. E.; U.S. Patent No. US20170089119A1. (2017). Milan, IT: U.S. Patent and Trademark Office.

[10] Frieling, B.; German Patent No. DE202016003231U. (2016). Vress, DE: Deutsche Patent- und Markenamt

[11] Teleky, W.; U.S. Patent No. US3715998A. (1971). West New York, NJ: U.S. Patent and Trademark Office.

[12] Walsh, M. J.; U.S. Patent No. US6044777A. (2000). Paso Robles, CA: U.S. Patent and Trademark Office.

[13] Brush, Jr.; John D.; U.S. Patent No. US4048926A. (1977). Webster, NY: U.S. Patent and Trademark Office.

[14] Harry, D. W., Sedlock, G. T., Vankirk, T. A., Kalinowski, J. M.; U.S. Patent No. US5970890A. (1999). North Canton, OH: U.S. Patent and Trademark Office.

[15] Harry, D. W., Sedlock, G. T., Vankirk, T. A., Kalinowski, J. M., Dunlap, R. E., Antram, H. E., Kalinowski, J. M., Mercer, S. A., Cox, P. J., Kontor, K. C., Graef, H. T.; U.S. Patent No. US6089168A. (2000). North Canton, OH: U.S. Patent and Trademark Office.

[16] Lankard, D. R.,Shoop, J. D.; U.S. Patent No. US4593627A. (1986). Canton, OH: U.S. Patent and Trademark Office.

[17] Wurster, H. J.; U.S. Patent No. US4377977A. (1983). Hamilton, OH: U.S. Patent and Trademark Office.

[18] Sands, R. L., Ward, G. M.; U.S. Patent No. US4389948A. (1983). London, GB: U.S. Patent and Trademark Office

[19] Lankard, D. R., Shoop, J. D.; U.S. Patent No. US4559881A. (1985). Canton, OH: U.S. Patent and Trademark Office

[20] Shoop, J. D., Graef, H. T., Newton, K. H., Grucza, S. M.; U.S. Patent No. US4615280A. (1986). Canton, OH: U.S. Patent and Trademark Office

[21] Taylor, K. M., Palicka, R. J.; U.S. Patent No. US3765300A. (1973). Niagara Falls, NY: U.S. Patent and Trademark Office

[22] Berman, C.; U.S. Patent No. US9562386B2. (2017). Mount Airy, NC: U.S. Patent and Trademark Office.

[23] Polensky, D.; U.S. Patent No. US5490468A. (1996). San Jose, CA: U.S. Patent and Trademark Office.

[24] Rabinowicz, E.; (1995). Friction and wear of materials. Second Edition. John Wiley & Sons, Inc. ISBN: 978-0-471-83084-9

[25] Moore, M. A. (1974). The relationship between the abrasive wear resistance, hardness and microstructure of ferritic materials. Wear, 28(1), 59-68.

[25] Ni, W., Cheng, Y. T., Lukitsch, M. J., Weiner, A. M., Lev, L. C., & Grummon, D. S. (2004). Effects of the ratio of hardness to Young's modulus on the friction and wear behavior of bilayer coatings. Applied physics letters, 85(18), 4028-4030.

[26] Standard Specification for High-Yield-Strength, Quenched and Tempered Alloy Steel Plate, Suitable for Welding, ASTM A514/A514M -14

[27] Xu, X., Xu, W., Ederveen, F. H., & van der Zwaag, S. (2013). Design of low hardness abrasion resistant steels. Wear, 301(1-2), 89-93.

[28] Dao, M., Lu, L., Asaro, R. J., De Hosson, J. T. M., & Ma, E. (2007). Toward a quantitative understanding of mechanical behavior of nanocrystalline metals. Acta Materialia, 55(12), 4041-4065.

[29] Leyland, A., & Matthews, A. (2000). On the significance of the H/E ratio in wear control: a nanocomposite coating approach to optimised tribological behaviour. Wear, 246(1-2), 1-11.

[30] Cheng, Y. T., & Cheng, C. M. (1998). Relationships between hardness, elastic modulus, and the work of indentation. Applied physics letters, 73(5), 614-616.

[31] Tönshoff, H. K., Peters, J., Inasaki, I., & Paul, T. (1992). Modelling and simulation of grinding processes. CIRP Annals-Manufacturing Technology, 41(2), 677-688.

[32] Kaczmarek, J. (2008). The effect of abrasive cutting on the temperature of grinding wheel and its relative efficiency. Archives of civil and mechanical engineering, 8(2), 81-91.

[33] Shaw, M. C. (1996). Energy conversion in cutting and grinding. CIRP Annals-Manufacturing Technology, 45(1), 101-104.

[34] Hosseini, A., & Kishawy, H. A. (2014). Cutting tool materials and tool wear. In Machining of titanium alloys (pp. 31-56). Springer, Berlin, Heidelberg.

[35] Kopac, J., & Krajnik, P. (2006). High-performance grinding—a review. Journal of Materials Processing Technology, 175(1-3), 278-284.

[36] Cambridge Materials EduPack, Granta Design Ltd, Cambridge, U.K.

[37] Lu, T. J., & Fleck, N. A. (1998). The thermal shock resistance of solids. Acta materialia, 46(13), 4755-4768.

[38] Panda, P. K., Kannan, T. S., Dubois, J., Olagnon, C., & Fantozzi, G. (2002). Thermal shock and thermal fatigue study of ceramic materials on a newly developed ascending thermal shock test equipment. Science and Technology of Advanced Materials, 3(4), 327-334.

[39] Fahrenwaldt, H. J., & Schuler, V. (2011). Praxiswissen schweisstechnik: werkstoffe, prozesse, fertigung. Springer-Verlag.

[40] A. L. BreiterV. M. Mal'tsevE. I. Popov (1977). Models of metal ignition. Combustion, Explosion and Shock Waves, Volume 13, Issue 4, pp 475–485

[41] Wang, H., Hlavacek, V., & Pranda, P. (2004). Model analysis of thermal lance combustion. Industrial & engineering chemistry research, 43(16), 4703-4708.

[42] Bolobov, V. I., & Berezin, A. Y. (1998). Conditions for ignition of copper and copper alloys in oxygen. Combustion, Explosion and Shock Waves, 34(2), 159-162.

[43] Yuasa, S., Zhu, Y., & Sogo, S. (1997). Ignition and combustion of aluminum in oxygen/nitrogen mixture streams. Combustion and Flame, 108(4), 387-396.

[44] Bolobov, V. I. (2001). Conditions for ignition of iron and carbon steel in oxygen. Combustion, Explosion and Shock Waves, 37(3), 292-296.

[45] Grosse, A. V., & Conway, J. B. (1958). Combustion of metals in oxygen. Industrial & Engineering Chemistry, 50(4), 663-672.

[46] Babrauskas, V. (1992). Related Quantities. Part A. Heat of Combustion and Potential Heat. Heat Release in Fires, 207-223.

[47] Baehr, H. D., & Stephan, K. (1996). Wärme-und Stoffübertragung (Vol. 2). Berlin Heidelberg New York: Springer.

[48] Xiaowei, L., Jean-Charles, R., & Suyuan, Y. (2004). Effect of temperature on graphite oxidation behavior. Nuclear Engineering and design, 227(3), 273-280.

[49] Zhang, Y. (2008). Geochemical kinetics. Princeton University Press.

[50] Windes, W., Strydom, G., Kane, J., & Smith, R. (2014). Role of nuclear grade graphite in controlling oxidation in modular HTGRs (No. INL/EXT--14-31720). Idaho National Lab.(INL), Idaho Falls, ID (United States).

[51] Gulbransen, E. A., Andrew, K. F., & Brassart, F. A. (1963). The oxidation of graphite at temperatures of 600 to 1500 C and at pressures of 2 to 76 torr of oxygen. Journal of the Electrochemical Society, 110(6), 476-483.

[52] Chiu, H. T., Chiu, S. H., Jeng, R. E., & Chung, J. S. (2000). A study of the combustion and fire-retardance behaviour of unsaturated polyester/phenolic resin blends. Polymer Degradation and Stability, 70(3), 505-514.

[53] Fitzer, E., & Schäfer, W. (1970). The effect of crosslinking on the formation of glasslike carbons from thermosetting resins. Carbon, 8(3), 353-364.

[54] Jiang, H., Wang, J., Wu, S., Yuan, Z., Hu, Z., Wu, R., & Liu, Q. (2012). The pyrolysis mechanism of phenol formaldehyde resin. Polymer degradation and stability, 97(8), 1527-1533.

[55] Aristizabal, M., Sanchez, J. M., Rodriguez, N., Ibarreta, F., & Martinez, R. (2011). Comparison of the oxidation behaviour of WC–Co and WC–Ni–Co–Cr cemented carbides. Corrosion Science, 53(9), 2754-2760.

[56] White, E. L., & Ward, J. J. (1966). Ignition of metals in oxygen (No. DMIC-224). BATTELLE MEMORIAL INST COLUMBUS OH DEFENSE METALS INFORMATION CENTER.

[57] Chen, L., Yi, D., Wang, B., Liu, H., & Wu, C. (2016). Mechanism of the early stages of oxidation of WC–Co cemented carbides. Corrosion Science, 103, 75-87.

[58] Pullar, R. C., Farrah, S., & Alford, N. M. (2007). MgWO4, ZnWO4, NiWO4 and CoWO4 microwave dielectric ceramics. Journal of the European Ceramic Society, 27(2-3), 1059-1063.

[59] Humphry-Baker, S. A., & Lee, W. E. (2016). Tungsten carbide is more oxidation resistant than tungsten when processed to full density. Scripta Materialia, 116, 67-70.

[60] Hertzberg, R. W., Vinci, R. P., Hertzberg J. L., (2013). Deformation and Fracture Mechanics of Engineering Materials (Fifth Edition). John Wiley & Sons, Inc.

[61] Weißbach, W. (2010). Werkstoffkunde: Strukturen, Eigenschaften, Prüfung. Springer-Verlag.

[62] Sierakowski, R. L. (1997). Strain rate behavior of metals and composites. In Convegno IGF XIII Cassino 1997.

[63] Stepanov, G. V., Zubov, V. I., Olisov, A. N., & Tokarev, V. M. (2000). Tensile strength of sheet materials under impact loading. Strength of materials, 32(4), 351-356.

[64] Huh, H., Lim, J. H., & Park, S. H. (2009). High speed tensile test of steel sheets for the stress-strain curve at the intermediate strain rate. International Journal of Automotive Technology, 10(2), 195-204.

[65] Roth, C. C., & Mohr, D. (2014). Effect of strain rate on ductile fracture initiation in advanced high strength steel sheets: experiments and modeling. International Journal of Plasticity, 56, 19-44.

[66] Hornbogen, E. (2006). Werkstoffe: Aufbau Und Eigenschaften Von Keramik-. Metall-, Polymer-Und Verbundwerkstoffen. 8., Bearbeitete Und Ergänzte Auflage Mit 338 Abbildungen Und 102 Tabellen. Springer.

[67] Frommeyer, G., Brüx, U., & Neumann, P. (2003). Supra-ductile and high-strength manganese-TRIP/TWIP steels for high energy absorption purposes. ISIJ international, 43(3), 438-446.

[68] Rossoll, A., Berdin, C., & Prioul, C. (2002). Determination of the fracture toughness of a low alloy steel by the instrumented Charpy impact test. International Journal of Fracture, 115(3), 205-226.

[69] Chao, Y. J., Ward Jr, J. D., & Sands, R. G. (2007). Charpy impact energy, fracture toughness and ductile–brittle transition temperature of dual-phase 590 Steel. Materials & design, 28(2), 551-557.

[70] Rösler, J., Harders, H., & Bäker, M. (2008). Mechanisches Verhalten der Werkstoffe (Vol. 3). Wiesbaden: Vieweg+ Teubner.

[71] Ahmed, M., Mallick, J., & Hasan, M. A. (2016). A study of factors affecting the flexural tensile strength of concrete. Journal of King Saud University-Engineering Sciences, 28(2), 147-156.

[72] Takahashi, Y. (1961). Viscoelastic properties of the phenolic resin–polyvinyl butyral system. Journal of Applied Polymer Science, 5(16), 468-477.

[73] Lou, D., Hellman, J., Luhulima, D., Liimatainen, J., & Lindroos, V. K. (2003). Interactions between tungsten carbide (WC) particulates and metal matrix in WC-reinforced composites. Materials Science and Engineering: A, 340(1-2), 155-162.